MBoC | ARTICLE

Activation of CWI pathway through high hydrostatic pressure, enhancing glycerol efflux via the aquaglyceroporin Fps1 in *Saccharomyces cerevisiae*

Takahiro Mochizuki[a,†], Toshiki Tanigawa[a,†], Seiya Shindo[a], Momoka Suematsu[a], Yuki Oguchi[b], Tetsuo Mioka[a], Yusuke Kato[a], Mina Fujiyama[a], Eri Hatano[a], Masashi Yamaguchi[c], Hiroji Chibana[c], and Fumiyoshi Abe[a,*]

[a]Department of Chemistry and Biological Science, and [b]Center for Instrumental Analysis, College of Science and Engineering, Aoyama Gakuin University, 5-10-1 Fuchinobe, Chuo-ku, Sagamihara 252-5258, Japan; [c]Medical Mycology Research Center, Chiba University, 1-8-1 Inohana, Chuo-ku, Chiba 260-8673, Japan

ABSTRACT **The fungal cell wall is the initial barrier for the fungi against diverse external stresses, such as osmolarity changes, harmful drugs, and mechanical injuries. This study explores the roles of osmoregulation and the cell-wall integrity (CWI) pathway in response to high hydrostatic pressure in the yeast *Saccharomyces cerevisiae*. We demonstrate the roles of the transmembrane mechanosensor Wsc1 and aquaglyceroporin Fps1 in a general mechanism to maintain cell growth under high-pressure regimes. The promotion of water influx into cells at 25 MPa, as evident by an increase in cell volume and a loss of the plasma membrane eisosome structure, activates the CWI pathway through the function of Wsc1. Phosphorylation of Slt2, the downstream mitogen-activated protein kinase, was increased at 25 MPa. Glycerol efflux increases via Fps1 phosphorylation, which is initiated by downstream components of the CWI pathway, and contributes to the reduction in intracellular osmolarity under high pressure. The elucidation of the mechanisms underlying adaptation to high pressure through the well-established CWI pathway could potentially translate to mammalian cells and provide novel insights into cellular mechanosensation.**

Monitoring Editor
Sophie Martin
Université de Genève

Received: Mar 10, 2023
Revised: May 26, 2023
Accepted: Jun 22, 2023

INTRODUCTION

Microorganisms encounter a wide variety of extreme environmental conditions, including heat, cold, salinity, or nutrient starvation. These stresses are first detected by sensor proteins that trigger the expression of specific genes via intracellular signaling pathways to respond to and overcome a crisis. Eukaryotes are also subjected to physical stresses including tension, shear forces, and hydrostatic pressure. In mammalian cells, forces are detected, at the cell surface, through specific classes of integral membrane receptors, such as integrins and cadherins, which transduce stimuli into biochemical signals that initiate adaptive responses (Ladoux and Mege, 2017; Kechagia *et al.*, 2019). Unlike stretching or expansion, hydrostatic pressure acts on cells as a uniform stress and affects all substances and reactions in the cell, according to Pascal's principle. Therefore, it is difficult to identify sensors of high hydrostatic pressure and determine their effects on complex intracellular signaling networks. Nevertheless, there is ample evidence that cells modify their metabolism, transcription, translation, or posttranslational processes in response to increasing hydrostatic pressure (Abe *et al.*, 1999; Iwahashi, 2015; Bourges *et al.*, 2017; Pattappa *et al.*, 2019; Hodder *et al.*, 2020; Abe, 2021; Mishra *et al.*, 2022).

Human cells also experience high hydrostatic pressures. In joints, cartilage is typically subjected to hydrostatic pressures between 3 and 10 MPa (0.1 MPa = 1 bar = 0.9869 atm = 1.0197 kg/cm^2) (Afoke *et al.*, 1987), with a maximum pressure of 18 MPa in the hip joint (Hodge *et al.*, 1989). The loading of endothelial cells with a low

This article was published online ahead of print in MBoC in Press (http://www.molbiolcell.org/cgi/doi/10.1091/mbc.E23-03-0086) on June 28, 2023.

†These authors contributed equally to this work.

Author contributions: T.M. and T.T., and F.A. conceptualized the study; T.M., T.T., S.S., M.S., Y.O., M.F., and E.H. investigated; T.M., Y.K., M.Y., H.C., and F.A. cooperated; F.A. supervised, wrote the original draft, reviewed and edited.

*Address correspondence to: Fumiyoshi Abe (abef@chem.aoyama.ac.jp).

Abbreviations used: CWI pathway, cell-wall integrity pathway; MPa, megapascals.

pressure of 50 mm Hg (~6.7 kPa) activates protein kinase C (Pkc1) and transiently activates the Ras/ERK pathway as a result of the water efflux through aquaporin 1 (Yoshino *et al.*, 2020). High-pressure adaptation mechanisms in deep-sea microorganisms have also received considerable attention. However, little is known regarding how microbial cells detect such stimuli and convert them to intracellular signals.

Although *Saccharomyces cerevisiae* (*S. cerevisiae*) is not a deep-sea piezophile, it can be used to elucidate the molecular mechanisms underlying the cell's responses to high hydrostatic pressure by applying basic knowledge of genetics and protein functions (Abe, 2021). Pressure pretreatment at a sublethal level (50 MPa for 1 h) increased the viability of yeast cells at 200 MPa, which is governed by two stress-induced transcription factors, Msn2 and Msn4 (Domitrovic *et al.*, 2006). High pressure of 25 MPa accumulates superoxide anions in mitochondria in a mutant deficient in superoxide dismutase 1, and the mutant shows marked sensitivity to high pressures (Funada *et al.*, 2022). Incubation of yeast cells at 25 MPa for 5 h resulted in the upregulation of the *DAN/TIR* family mannoprotein genes, which are induced under hypoxic conditions and at low temperatures (Abe, 2007). Target of rapamycin complex 1 (TORC1), an evolutionarily conserved serine/threonine kinase in eukaryotes, was activated by a pressure of 25 MPa (Uemura *et al.*, 2020). We demonstrated that TORC1 plays a critical role in maintaining an appropriate glutamine level under high pressure by downregulating the de novo synthesis of glutamine (Uemura *et al.*, 2020). Such evidence indicates that high-pressure stress induces diverse changes in intracellular processes and that cells survive by adaptively coping with each change. Moreover, yeast species have been found in deep-sea sediments thousands of meters below the ocean surface as well as in the bodies of deep-sea organisms (Abe *et al.*, 2006; Bass *et al.*, 2007; Nagahama *et al.*, 2008; Burgaud *et al.*, 2015), suggesting that certain yeast species are naturally adapted to and capable of surviving under high-pressure conditions.

The fungal cell wall provides the first barrier against external stresses, such as osmolarity changes, harmful drugs, and mechanical injuries. It is an elastic structure with a thickness of 50–500 nm and is composed of β1,3-glucan, β1,6-glucan, chitin, and mannoproteins (Lesage and Bussey, 2006; Levin, 2011; Orlean, 2012). The Young's modulus of the cell wall is estimated to be between 10 and 100 MPa (Ma *et al.*, 2005; Davi *et al.*, 2019), which is an intermediate value between that of low-density polyethylene and rubber. The primary mechanical role of the cell wall is to maintain cell morphology by balancing the tension generated by the turgor pressure, which is important for polarized cell growth (Madden and Snyder, 1998; Pruyne and Bretscher, 2000; Bi and Park, 2012). In *S. cerevisiae*, cell-wall destabilization is sensed by transmembrane sensors of the WSC family (Wsc1, Wsc2, and Wsc3), as well as Mid2 and its homologue Mtl1 (Philip and Levin, 2001; Levin, 2005; Levin, 2011; Kock *et al.*, 2015; Jimenez-Gutierrez *et al.*, 2020), which activates a conserved signal-transduction cascade, namely, the cell-wall integrity (CWI) pathway. Their architecture is analogous to that of the mammalian transmembrane integrins (Elhasi and Blomberg, 2019). Among the five sensor proteins in *S. cerevisiae*, Wsc1 has been extensively studied both genetically and biophysically (Philip and Levin, 2001; Merchan *et al.*, 2004; Dupres *et al.*, 2009; Heinisch *et al.*, 2010; Banavar *et al.*, 2018; Neeli-Venkata *et al.*, 2021; Schoppner *et al.*, 2022). The CWI pathway in *S. cerevisiae* is activated in response to cell-wall damage; however, recent evidence suggests that it is also involved in other stress conditions, indicating functional diversity (Straede and Heinisch, 2007; Cruz *et al.*, 2013; Kock *et al.*, 2016; Banavar *et al.*, 2018). To date, the effects of high hydrostatic pressure in yeast cells have not been studied with a focus on osmoregulation and the CWI pathway.

Atomic force microscopy (AFM) analysis revealed that a serine-threonine-rich (STR) domain has a nanospring-like structure that expands and contracts under external pressure, which in turn causes dephosphorylation of the cytoplasmic tail of Wsc1, transmitting signals downstream (Vay *et al.*, 2004; Dupres *et al.*, 2009; Heinisch *et al.*, 2010). The cytoplasmic tail of Wsc1 interacts with the GDP/GTP exchange factor Rom2, which subsequently activates small GTPase Rho1(Philip and Levin, 2001; Vay *et al.*, 2004). Bem2, Sac7, Lrg1, and Bag7 act as GTPase-activating proteins (GAPs) for Rho1 (Peterson *et al.*, 1994; Schmidt *et al.*, 1997; Martin *et al.*, 2000; Schmidt *et al.*, 2002). Rho1 regulates Pkc1, a serine/threonine protein kinase that is essential for cell-wall remodeling (Figure 1) (Levin, 2011). Pkc1 then activates three protein-kinase-signaling modules that integrate the mitogen-activated protein kinase kinase kinase (MAPKKK) Bck1, redundant mitogen-activated protein kinase kinases (MAPKKs) Mkk1 and Mkk2, and mitogen-activated protein kinase (MAPK) Slt2 (Levin, 2011). Slt2 kinase regulates many cellular processes, such as fine-tuning of the CWI pathway, transcriptional response to cell-wall damage, cell-cycle progression, and nuclear export of mRNA (Gonzalez-Rubio *et al.*, 2022), and mediates aquaglyceroporin Fps1 phosphorylation (Levin, 2005; Mollapour *et al.*, 2009; Ahmadpour *et al.*, 2016). Although the CWI cascade is well characterized (Figure 1), the exact mode of Wsc1 action in response to different environmental cues remains unclear.

Fps1 is under the control of the CWI pathway (Ahmadpour *et al.*, 2016; Laz *et al.*, 2020). In yeast, when the cell wall is damaged, water flows into the cell owing to the osmotic pressure difference between the inside and outside of the cell. To cope with this stress and prevent osmolysis, yeast cells activate Fps1 to expel glycerol and eliminate osmotic pressure differences (Tamas *et al.*, 1999). The opening and closing of Fps1 is a complex process mediated by protein phosphorylation involving several signaling pathways (Figure 1). First, MAP kinase Hog1 is activated in response to hyperosmotic stress and phosphorylates the T231 residue of Fps1, resulting in Fps1 closure (Thorsen *et al.*, 2006; Mollapour and Piper, 2007). Hog1 negatively regulates this channel by displacing the Fps1-activating proteins Rgc1 and Rgc2, thereby causing Fps1 closure (Lee *et al.*, 2013). Second, the open state of Fps1 requires phosphorylation by Ypk1, a target of TORC2-dependent protein kinase (Muir *et al.*, 2015). Third, Fps1 and Slt2 physically interact via phosphorylation of the S537 residue of Fps1, which promotes the opening of the glycerol channel (Ahmadpour *et al.*, 2016).

Remarkably, while imaging wild-type *S. cerevisiae* cells, minor cell swelling was observed after high-pressure incubation at 25 MPa. This suggests that high pressure may facilitate the influx of water into the cell or damage the cell wall, further allowing water influx. This observation steered us to study high-pressure signaling, with a focus on water influx, turgor pressure, the CWI pathway via Wsc1, MAP kinase Slt2, and aquaglyceroporin Fps1 (Figure 1). Our study provides novel insights into the signaling events triggered by the application of high hydrostatic pressure and the resulting molecular mechanisms that help cells to cope with such stress.

RESULTS

Wsc1 is required for efficient cell growth under high pressure

Based on the previous studies (Philip and Levin, 2001; Levin, 2005; Levin, 2011; Kock *et al.*, 2015; Jimenez-Gutierrez *et al.*, 2020), we hypothesized that any of the five sensor proteins, Wsc1–3, Mid2, and Mtl1, could detect hydrostatic pressure changes, either directly

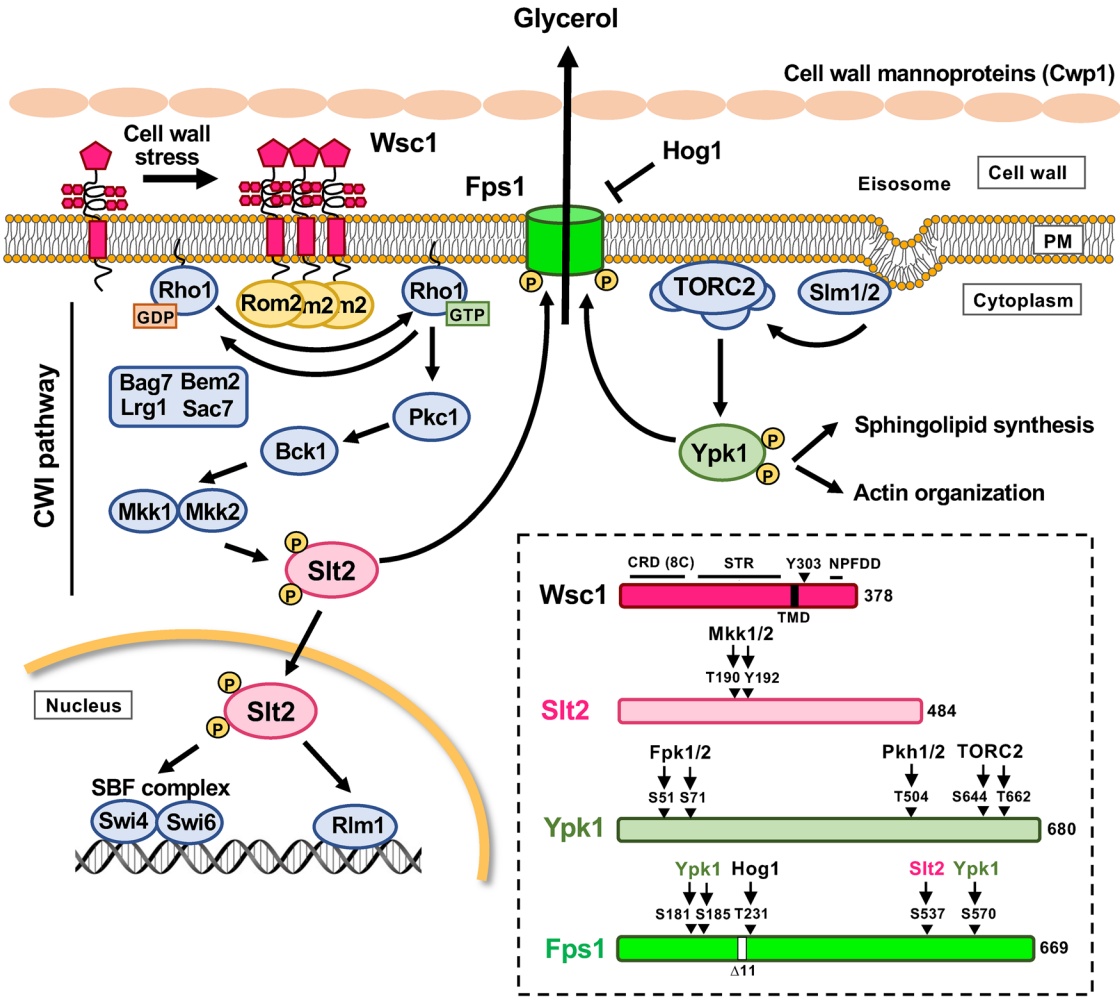

FIGURE 1: Schematic representation of the CWI pathway in *S. cerevisiae*. Five cell-wall sensor proteins are depicted. Upon cell-wall stress, Wsc1 first clusters at the cell surface. Binding of the GDP/GTP exchanging factor, Rom2, to the cytoplasmic tail of Wsc1 activates the small GTPase, Rho1. Rho1-GTP activates the Pkc1, which activates a conserved mitogen-activated protein kinase (MAPK) cascade. The cascade consists of Bck1 (MAPKKK), Mkk1/Mkkk2 (MAPKKs), and Slt2 (MAPK). Phosphorylated Slt2 (P-Slt2) translocates into the nucleus and promotes cell cycle progression through the SBF complex and transcription of genes encoding cell-wall proteins by Rlm1. Slt2 also phosphorylates the aquaglyceroporin, Fps1, and promotes Fps1 opening to expel glycerol. When cells are stressed, tension is applied to the plasma membrane, causing the loss of the eisosome, a plasma membrane invaginating structure. Slm1/Slm2 localized in the eisosome migrate to TORC2. Consequently, TORC2 is activated and phosphorylates Ypk1. Phosphorylated Ypk1 also phosphorylates Fps1, positively regulating glycerol efflux. The phosphorylation sites, kinases, and functional motifs in major proteins used in this study are outlined below. CRD (8C), CRD (C27, C49, C53, C69, C71, C86, C90, and C98); STR, serine/threonine-rich domain (111–265 amino acid residues); NPFDD motif, N344-P345-F346-D347-D348.

or as a result of cell-wall damage, and activate the CWI pathway to allow for high-pressure growth. Figure 2 illustrates the experimental setup for high-pressure experiments. To examine cell growth, exponentially growing cells in synthetic complete (SC) medium were diluted with the same medium to an initial OD_{600} of 0.01 and then exposed to either atmospheric pressure (0.1 MPa) or high pressure (5–30 MPa). We found that the *wsc1*Δ mutant exhibited a moderate growth defect at 25 MPa, whereas the other mutants grew as efficiently as the wild-type cells (Figure 3A). The result suggests that Wsc1 plays a primary role in high-pressure growth, while the other sensor proteins may contribute to the growth with overlapping functions.

Wsc1 is characterized by an N-terminal extracellular cysteine-rich domain (CRD), followed by a glycosylated STR domain, a single transmembrane domain, and a C-terminal cytoplasmic tail (Figure 1). The CRD and STR domains detect structural changes in the cell wall (Dupres *et al.*, 2009; Heinisch *et al.*, 2010). An alanine substitution of eight cysteines in the CRD of Wsc1 had a marginal effect on high-pressure growth ability, whereas deletions of the STR and the entire N-terminal region caused sensitivity to high pressure (Figure 3B). These results suggest that the STR of Wsc1 detects structural changes in the cell wall caused by high pressure.

Single-molecule AFM results indicated that Wsc1 assembles in patches as large as 200 nm on the plasma membrane, thereby enhancing transduction of the CWI signaling pathway (Dupres *et al.*, 2009; Heinisch *et al.*, 2010). Wsc1 assembles at the tips and bud necks where cells undergo polar growth, and endocytosis is essential for their polarity (Piao *et al.*, 2007). To determine the effect of

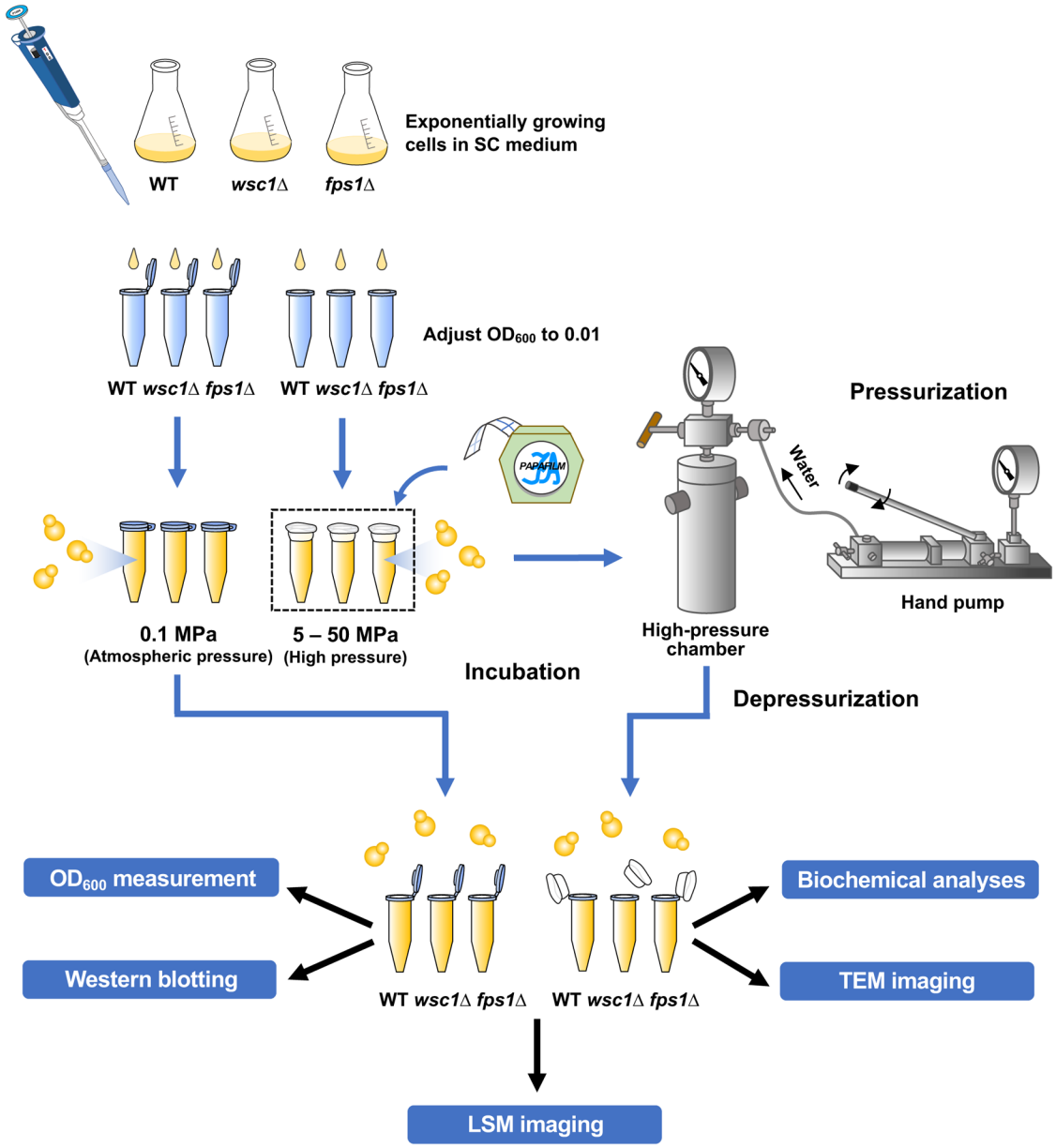

FIGURE 2: Experimental setup for high-pressure experiments. To quantitatively examine growth, exponentially growing cells in the SC medium were diluted to an initial OD_{600} of 0.01 with the same medium. Subsequently, the cells were exposed to either atmospheric pressure (0.1 MPa) or high pressure (5–30 MPa). Except for cell growth examination, different values were set for the initial OD_{600}, pressure intensity, and duration of high-pressure exposure.

high pressure on the distribution of Wsc1, we observed the localization of Wsc1-GFP before and after culturing the cells at 25 MPa for 5 h. Cells were observed after depressurization. As previously reported (Piao *et al.*, 2007; Wilk *et al.*, 2010), Wsc1-GFP localized primarily to small buds and the neck in large-budded cells (Figure 3C). However, it is also found in the plasma membrane of mother cells as patchy structures, and possibly in late endosomes as punctate structures and vacuoles (Figure 3C). The small bud and neck localization of Wsc1-GFP was maintained after the high-pressure incubation (Figure 3C). The overall localization of GFP-tagged $Wsc1^{8C>A}$, $Wsc1^{STR\Delta}$, and $Wsc1^{Nter\Delta}$ was comparable with that of the wild-type Wsc1-GFP (Figure 3C). The polarized distribution of Wsc1 to bud tips relies on endocytosis, which in turn requires the presence of the NPFDD motif in the C-terminal tail of the Wsc1 protein (Piao *et al.*, 2007; Wilk *et al.*, 2010). The Wsc1 mutant, in which the NPF sequence was replaced by AAA, exhibited a uniform distribution of Wsc1 within the plasma membrane (Piao *et al.*, 2007). $Wsc1^{NPF>AAA}$-GFP was present throughout the plasma membrane (Figure 3C) and $Wsc1^{NPF>AAA}$ expressing cells grew as efficiently as the wild-type cells at 25 MPa (Figure 3B). Therefore, we suggest that Wsc1 is required for efficient cell growth under high pressure but does not need to be exclusively localized to the bud tips.

Wsc1 is required for the full activation of CWI pathway in response to high pressure

To address the role of Wsc1 in optimal growth under high pressure, we focused on the downstream effector Rom2. The Wsc1 C-terminal cytoplasmic domain residue, Y303, is critical for its interaction with Rom2 (Vay *et al.*, 2004). Both the disruption of *ROM2* and the Wsc1-Y303A mutation, which interferes with the Wsc1–Rom2

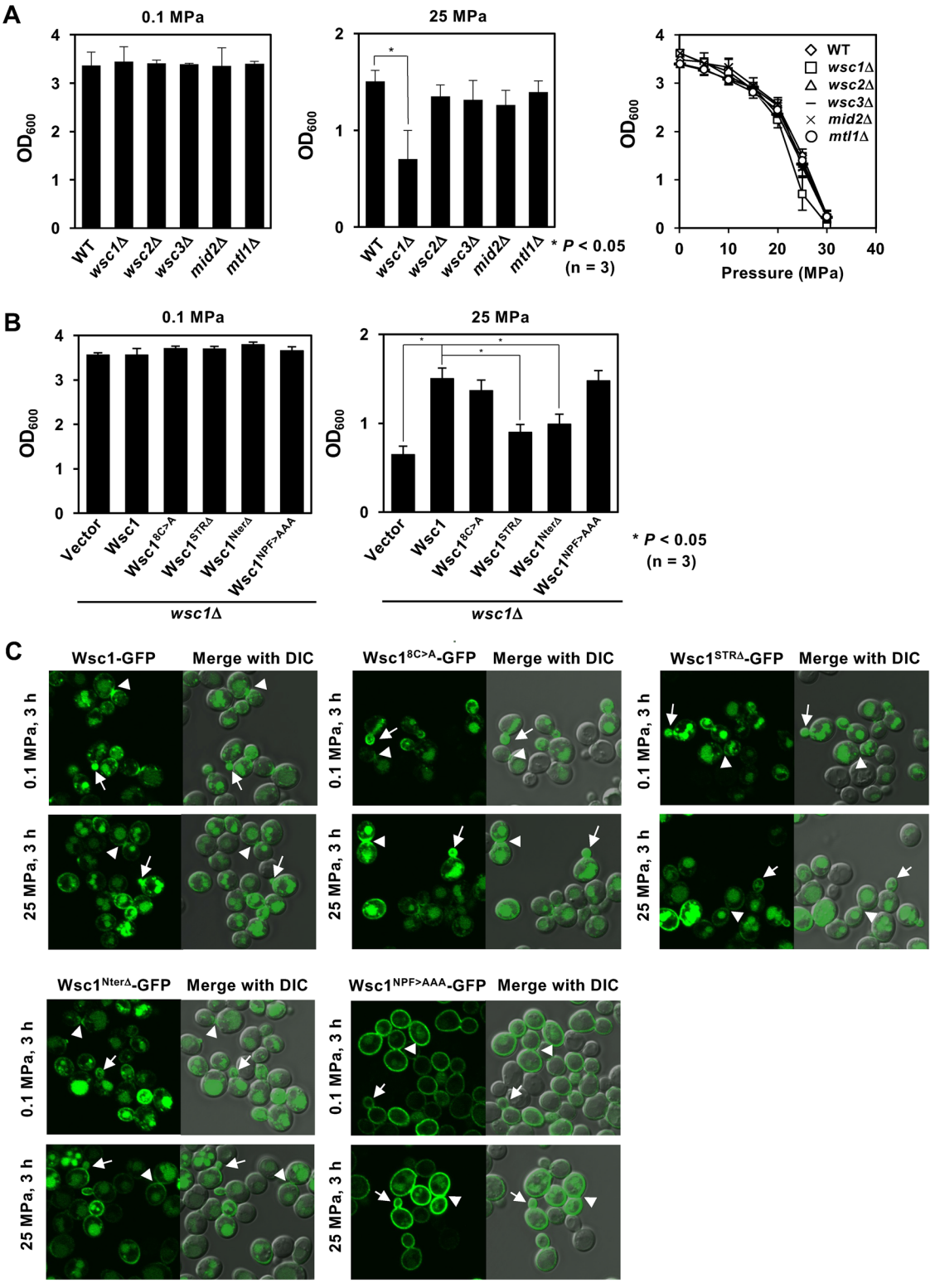

FIGURE 3: Wsc1 is required for growth under high pressure. (A) Wild-type and mutant cells were cultured in SC medium at 0.1 MPa or indicated pressures for 48 h with an initial OD_{600} = 0.01. (B) Cells with mutations in the extracellular domain of Wsc1 or the NPF>AAA substitution were cultured in SC medium at 0.1 or 25 MPa. Data are presented as mean ± SD of three independent experiments. (C). Wild-type cells expressing Wsc1-GFP or the mutant forms were cultured at 0.1 or 25 MPa for 3 h and were observed under a confocal laser microscope immediately after depressurization. Arrows and arrowheads indicate small buds and the neck in large-budded cells, respectively.

interaction, resulted in growth defects at 25 MPa (Figure 4A). Among the four Rho1 GAP genes, deletions in *BEM2, SAC7*, and *LRG1* caused growth defects at 25 MPa to varying degrees (Figure 4A). The expression of GTP-bound active forms of Rho1-F35L or Q68H (Yoshida *et al.*, 2009) failed to restore the high-pressure sensitivity of the *rom2*Δ mutant (Figure 4B), suggesting that the association of

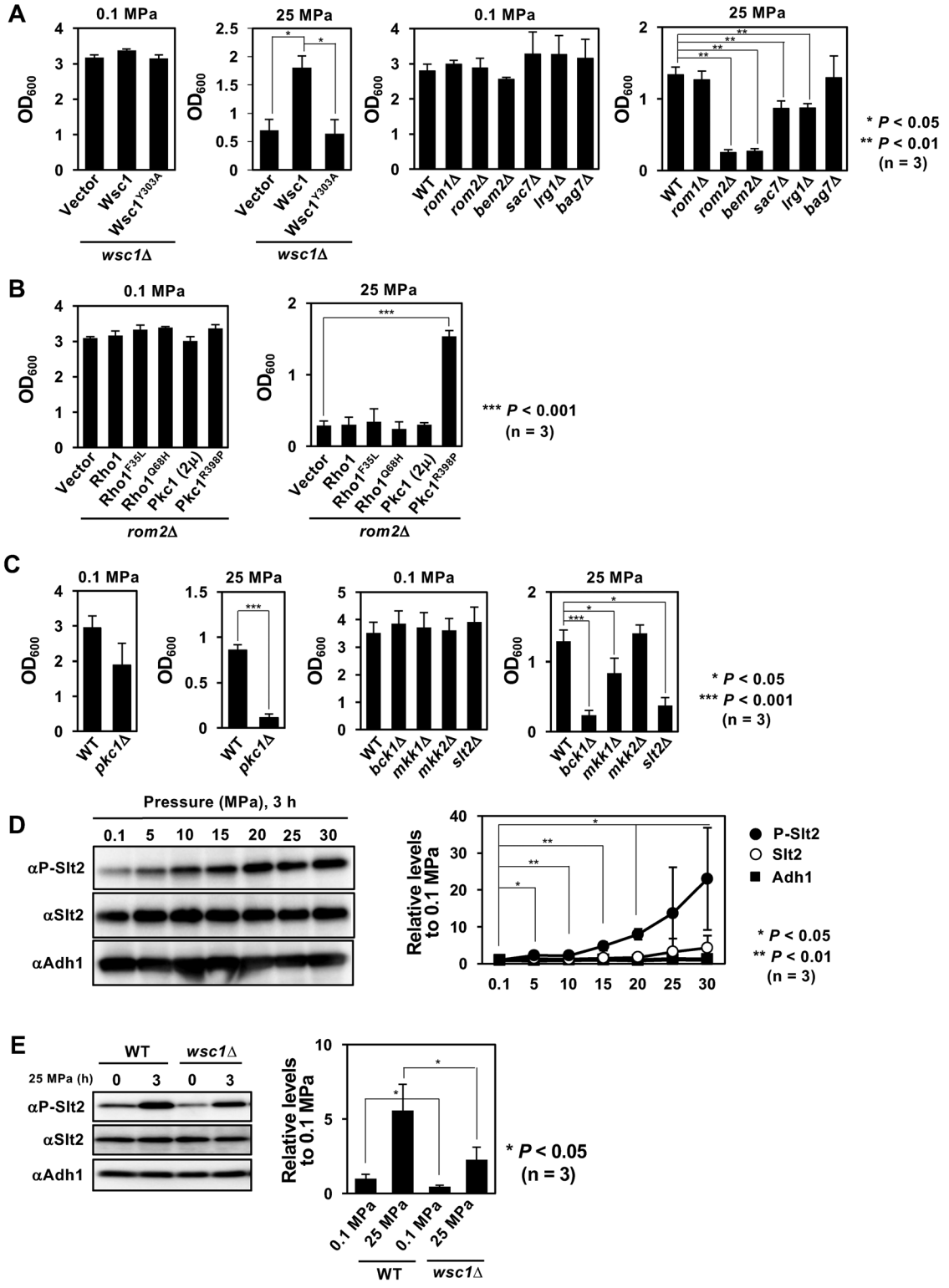

FIGURE 4: CWI pathway is activated by high pressure. (A) Mutant strains with various defects in the CWI pathway were cultured in SC medium at 0.1 or 25 MPa. (B) *rom2*Δ cells expressing Rho1 or Pck1 derivatives were cultured in SC medium at 0.1 or 25 MPa. (C) Mutant strains with various defects in the CWI pathway were cultured in SC medium at 0.1 or 25 MPa. Strains DL100 and DL376 harboring YCplac22 (*TRP1* and *CEN*) were used to examine the *PKC1* deficiency (left). (D) Wild-type cells were cultured in SC medium under various pressure conditions for 3 h. Slt2 and P-Slt2 were detected using Western blotting using specific antibodies. The relative intensities, P-Slt2/Adh1 and Slt2/Adh1, were quantified in an ImageQuant LAS4000 mini. (E) Wild-type or *wsc1*Δ cells were cultured in SC medium at 0.1 or 25 MPa for 3 h. Western blotting was performed as in (D). Data are presented as mean ± SD of three independent experiments.

Rho1 with Rom2 is critically important for high-pressure growth. The expression of the constitutively active form of Pkc1-R398P (Nonaka *et al.*, 1995) allowed the *rom2*Δ mutant to grow efficiently at 25 MPa (Figure 4B). Disruption of *PKC1*, *BCK1*, or *SLT2* resulted in severe high-pressure sensitivity, whereas disruption of only *MKK1*, and not *MKK2*, caused moderate high-pressure sensitivity (Figure 4C). These findings indicate that Wsc1 is essential for sensing alterations in hydrostatic pressure and potentially facilitating the transmission of pressure signal through the CWI pathway.

To confirm this hypothesis, we investigated the phosphorylation level of Slt2 under high pressure. The result demonstrated a pressure-dependent increase in Slt2 phosphorylation, indicating that high pressure indeed triggers the activation of the CWI pathway (Figure 4D). In addition, the disruption of *WSC1* reduced the phosphorylation level of Slt2 by 60% at 25 MPa compared with the wild-type level. This indicates that other proteins, such as Mid2, may also activate the CWI pathway in response to high pressure (Figure 4E). However, in the *wsc1*Δ strain, the basal level of Slt2 phosphorylation at 0.1 MPa was also reduced by 55% of the wild-type level (Figure 4E). Therefore, it is difficult to conclusively determine that Wsc1 triggers the activation of the CWI pathway in response to high pressure. It is possible that the high-pressure conditions also influenced the components of the CWI cascade, including Rom2, Rho1, or downstream kinases, resulting in the enhancement of Slt2 phosphorylation. This suggests that the effect of high pressure on Slt2 phosphorylation may be mediated indirectly through these components, rather than directly impacting the structural integrity of Wsc1 itself. Nevertheless, Wsc1 is essential for this process to occur effectively. Therefore, we performed several experiments regarding the downstream factors of Slt2.

Slt2 is regulated by the CWI signaling pathway, which is responsible for maintaining cell-wall homeostasis (Martin *et al.*, 2000; Levin, 2005; Gonzalez-Rubio *et al.*, 2022). Thus, increased Slt2 phosphorylation may modulate the transcription of downstream genes by phosphorylating its substrates under high pressure. Two transcription factors, Rlm1 and SBF (Swi4/Swi6), are activated by this pathway (Levin, 2011). To verify their necessity in high-pressure growth, we cultured each mutant strain at 25 MPa. The *rlm1*Δ mutant exhibited growth similar to the wild-type strain, whereas the *swi4*Δ and *swi6*Δ mutants displayed significant high-pressure sensitivity (Figure 5A). Therefore, it can be inferred that Swi4/Swi6, acting as downstream transcription factors of Slt2, play a vital role in high-pressure growth. Subsequently, we aimed to examine whether high pressure affects the phosphorylation levels of Swi4, Swi6, and Rlm1 by using SDS–PAGE mobility shift in Western blotting. However, when the wild-type strain was cultured at 25 MPa for 1–5 h, there was a significant decrease in the expression levels of Swi4-3HA and Swi6-3HA, and their high- and low-molecular-weight bands could not be distinguished (Figure 5B). Additionally, the band corresponding to Rlm1-3HA could not be detected.

Therefore, we examined the impact of high pressure on the subcellular localization of Swi4 and Swi6. Wild-type cells expressing Swi6-GFP were incubated with 15 μg/ml nocodazole in YPD medium for 2 h at 0.1 MPa to induce cell cycle arrest in the G_2/M phase when most of the Swi6-GFP was present in the cytoplasm (Kim *et al.*, 2010). SC medium was not used in this analysis because nocodazole was ineffective in arresting the cell cycle even at high concentrations (unpublished data). The cells were then cultured for 5 h under 0.1 or 25 MPa. We found that the percentage of cells with Swi6-GFP migrating from the cytoplasm to the nucleus was higher at 25 MPa (45%, $n > 300$) than at 0.1 MPa (22%, $n > 300$) (Figure 5C). Furthermore, similar results were obtained for Swi4-GFP (Figure 5C), which had not been previously reported for stress-induced nuclear translocation. Swi6 is known to translocate to the nucleus within 20 min after shifting cells to a high temperature of 39°C, followed by a gradual return to the cytoplasm after 40 min under high-temperature conditions (Kim *et al.*, 2010). In contrast, both Swi6 and Swi4 translocated to the nucleus within 5 h after shifting cells to 25 MPa (Figure 5C), while no nuclear translocation of Swi4 and Swi6 was observed when exposed to 25 MPa for only 1 h (our unpublished observation). This gradual nuclear translocation correlates with the observed increase in Slt2 phosphorylation levels, which occurs approximately 3 h after shifting to 25 MPa (Figure 4D).

To evaluate the activation of Rlm1 by Slt2, we investigated the transcriptional activity of Rlm1-responsive promoters for *SLT2*, *MLP1*, and *YIL117C* (Jung *et al.*, 2002) in response to high pressure. Cells harboring *lacZ* reporter plasmids were exposed to 25 MPa for 5 h. Subsequently, the β-galactosidase activity was quantified using the chromogenic substrate 2-Nitrophenyl-β-D-galactopyranoside (ONPG). Jung *et al*. (2002) performed the *lacZ* reporter assay using YPD medium and reported that the addition of calcofluor white (CFW) led to more than 10fold increase in the transcription of *SLT2*, *MLP1*, and *YIL117C*. In our experiment, we used SC medium; however, despite applying high pressure or adding CFW as a positive control, we did not observe any transcriptional induction of these genes (unpublished data). Hence, we also used YPD medium. Our findings demonstrated that high-pressure treatment did not lead to transcriptional activation of these genes, whereas CFW strongly enhanced transcription of *SLT2* and *YIL117C* (Figure 5D). These results suggest that Rlm1 may not function downstream of Slt2 in this context.

High pressure facilitates water influx into the cells

While performing this study, we noticed that the wild-type cells were moderately swollen after incubation at 25 MPa. To validate this further, we examined whether the distribution of eisosomes was affected by pressure. Eisosomes, peripheral-membrane protein complexes located on the cytoplasmic side of membrane compartments occupied by Can1 (MCC), are membrane invaginations (Douglas and Konopka, 2014; Lanze *et al.*, 2020; Sakata *et al.*, 2022). If the cell swells and the plasma membrane undergoes stretching under high pressure, the membrane invaginations should disappear. To verify this, we observed cells coexpressing the low-affinity tryptophan permease Tat1-GFP as a plasma membrane marker (Suzuki *et al.*, 2013; Ishii *et al.*, 2022) and an eisosome resident protein, Nce102-mCherry, after culturing at 25 or 50 MPa. Cells were observed at 0.1 MPa within 15 min of depressurization. At 0.1 MPa, Nce102-mCherry was localized to the plasma membrane in a patchy pattern characteristic of eisosomes (Figure 6A). Notably, after high-pressure culture at 25 or 50 MPa, Nce102-mCherry was evenly distributed within the plasma membrane (Figure 6A). This was partially suppressed by the presence of 1 M sorbitol (Figure 6A). When the colocalization of Tat1-GFP and Nce102-mCherry was examined at the cell surface, Pearson's correlation coefficient (PCC) increased with incubation time at 25 MPa (Figure 6B), confirming the even distribution of Nce102 under high pressure. Similar increases in PCC with Tat1 were found for Pil1 and Sur7, another two eisosome-associated proteins, but not as pronounced as for Nce102 (Figure 6B). These results suggest that the influx of water into the cells after high-pressure incubation results in tension in the plasma membrane.

Next, the cell volume was calculated by measuring the cell diameter using Tat1-GFP as the plasma membrane marker. We found that the cell volume increased 1.2fold after incubation at 25 MPa or

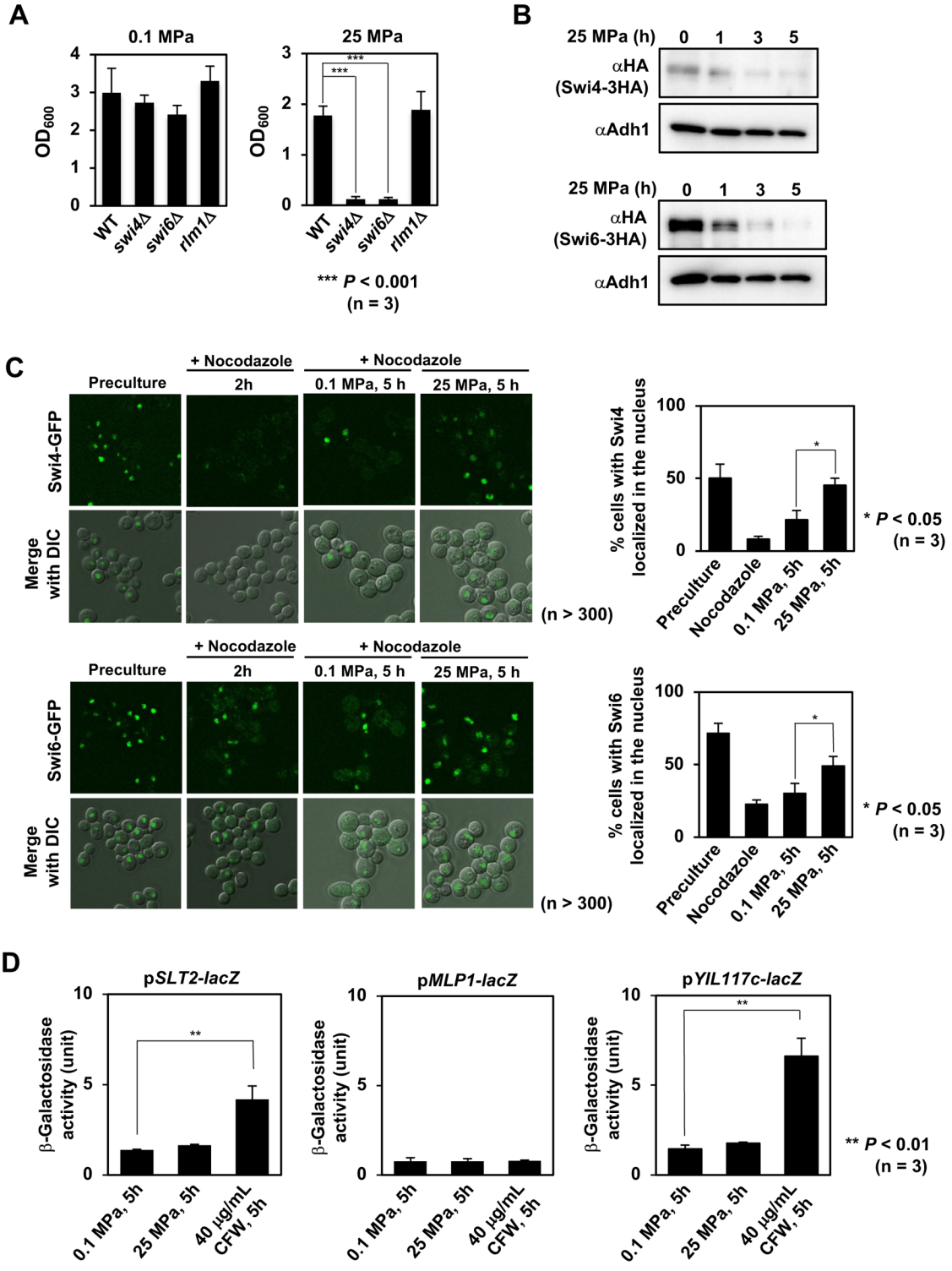

FIGURE 5: High pressure promotes nuclear translocation of Swi4 and Swi6. (A) Mutant strains were cultured in SC medium at 0.1 or 25 MPa. (B) Wild-type cells expressing Swi4-3HA or Swi6-3HA were cultured in SC medium at 0.1 or 25 MPa for 1–5 h. The cells were subjected to Western blotting. (C) Wild-type cells expressing Swi4-GFP or Swi6-GFP were incubated with 15 μg/ml nocodazole in YPD medium for 2 h at 0.1 MPa. The cells were then cultured for another 5 h at 0.1 or 25 MPa and were observed after depressurization. The percentages of cells with Swi4-GFP or Swi6-GFP in the nucleus in mt300 cells are shown. (D) Cells harboring the *lacZ* reporter plasmid were cultured in SC medium at 0.1 or 25 MPa for 5 h. β-galactosidase reporter assay was performed as described previously (Mochizuki *et al.*, 2015). Data are presented as mean ± SD of three independent experiments.

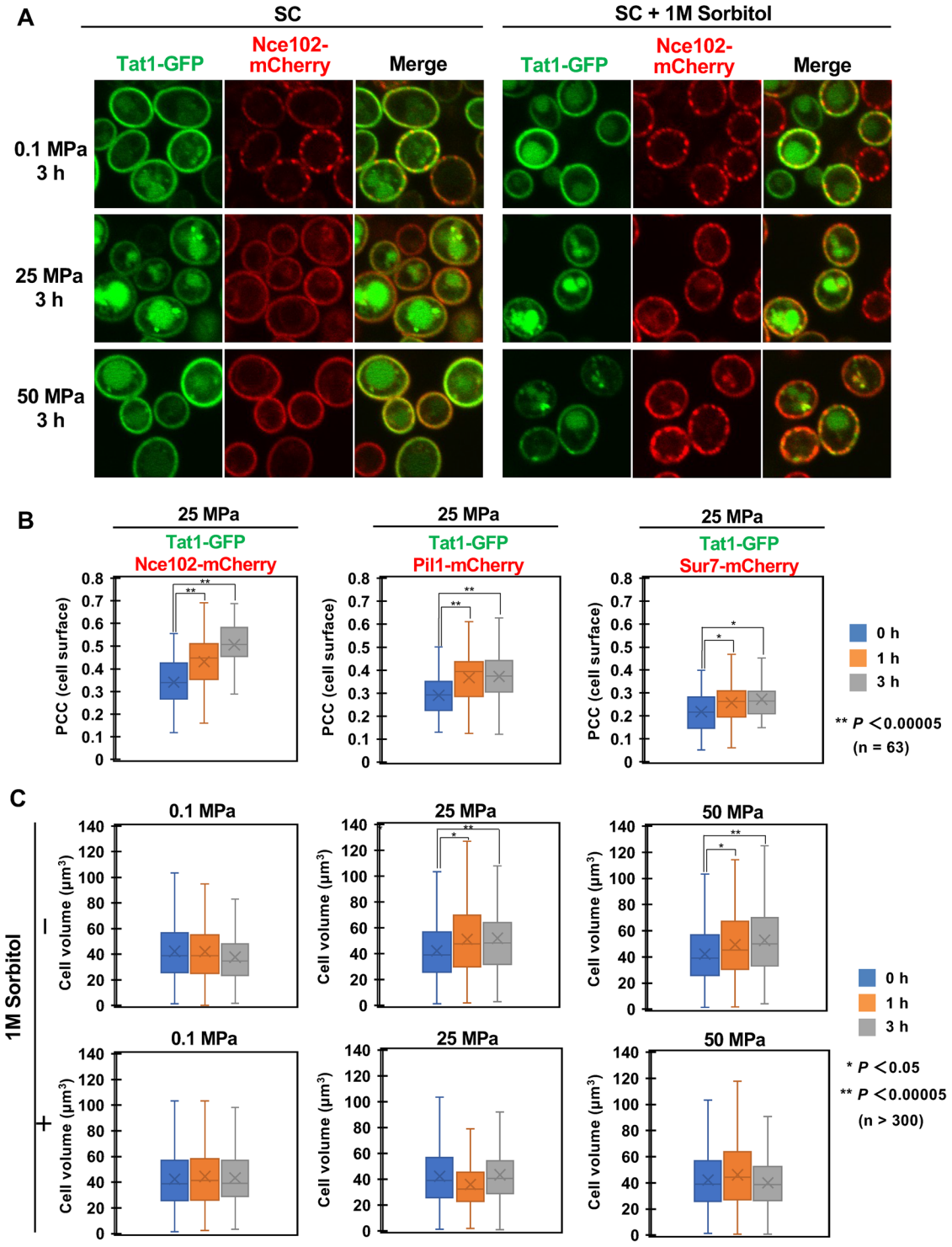

FIGURE 6: High pressure causes cell swelling and loss of the eisosome structure. (A) Wild-type cells coexpressing Tat1-GFP (plasma membrane marker) and Nce102-mCherry (eisosome marker) were cultured in SC medium at 0.1, 25, or 50 MPa for 3 h. After depressurization, cells were observed at 0.1 MPa under the confocal laser microscope. Cross-section images are shown. (B) Cells coexpressing Tat1-GFP and Nce102-mCherry, Pil1-mCherry, or Sur7-mCherry were cultured in SC medium at 0.1 or 25 MPa for 1 or 3 h. PCC was obtained for cell surface images from 63 cells in three independent experiments. (C) Changes in cell volume when cultured under high pressure. Cells were cultured at 0.1, 25, or 50 MPa for 1 or 3 h in SC medium with or without 1-M sorbitol. The cell volume was calculated from the cell diameter of mt300 cells after depressurization in three independent experiments.

50 MPa for 1 or 3 h, suggesting that water influx occurred under high pressure (Figure 6, A and B). To verify pressure-induced cell swelling, we examined the effects of 1 M sorbitol addition on cell volume under high pressure. As expected, 1 M sorbitol suppressed the high-pressure-induced increase in cell volume (Figure 6C). If high pressure merely pushed water into cells, the cell size would be

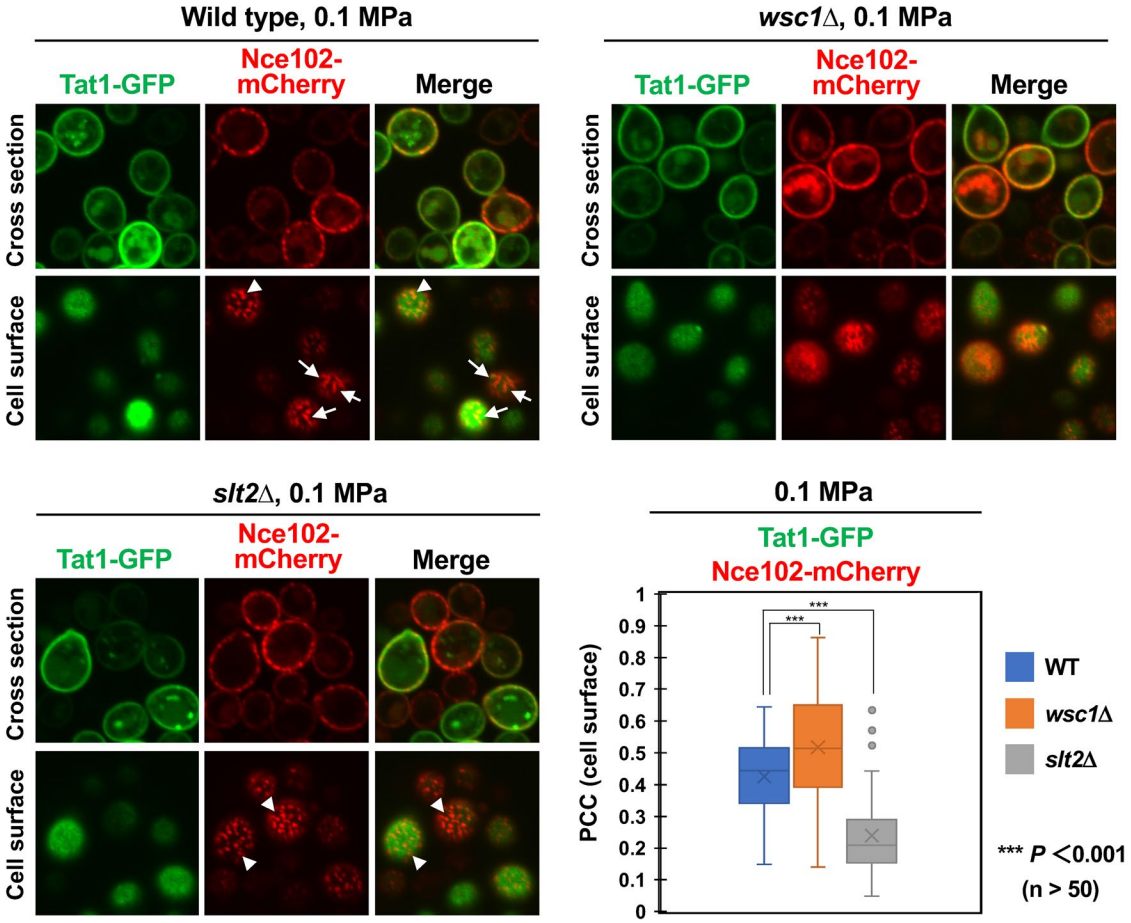

FIGURE 7: Eisosome structure in the *wsc1*Δ and *slt2*Δ mutants. Cells coexpressing Tat1-GFP and Nce102-mCherry were cultured in SC medium at 0.1 MPa and observed under the confocal laser microscope. PCC was obtained for cell surface images from mt50 cells of each strain in three independent experiments.

restored following depressurization. However, the above results show that the cells remain swollen 15 min post depressurization until microscopic observation at atmospheric pressure. Therefore, even 1 h of incubation at 25 or 50 MPa would have caused irreversible changes to the cell wall. However, it remains unclear whether a high-pressure load directly weakens the cell-wall structure, or the cell wall expanded irreversibly owing to the increased water influx into the cell due to high-pressure application.

Remarkably, the *wsc1*Δ mutant displayed a distinct pattern of Nce102-mCherry localization within the plasma membrane, diverging from the wild-type strain (Figure 7). Instead of the anticipated patchy distribution, Nce102-mCherry exhibited a more uniform distribution, even under 0.1 MPa, leading to an increased PCC with Tat1-GFP (Figure 7). This suggests an excessive water influx in the *wsc1*Δ mutant under the normal growth condition. In contrast to expectations, the *slt2*Δ mutant exhibited a reduced PCC between Nce102-mCherry and Tat1-GFP compared with the wild-type strain (Figure 7). We observed that the eisosome structures in the wild-type strain exhibited both furrow-like invaginations and dot-like formations (Figure 7, arrows and arrowheads, respectively) as reported previously (Stradalova *et al.*, 2009), whereas the eisosomes in the *slt2*Δ mutant predominantly displayed prominent dot-like structures (Figure 7, arrowheads). Therefore, the *slt2*Δ mutant has a reduced eisosome area compared with the wild-type strain, resulting in the decreased PCC. The exact cause of the eisosome shape changes resulting from the absence of Slt2 is currently unknown. In any case, cells faced an increased risk of rupture under high pressure. To counteract this, cells tend to prevent water influx by expelling glycerol, the primary osmolyte in yeast, to reduce internal osmotic pressure. Consequently, our focus was directed towards investigating the regulation of intracellular glycerol levels in response to high hydrostatic pressure.

Aquaglyceroporin Fps1-mediated glycerol efflux is required for high-pressure growth

Under hyperosmotic conditions, yeast cells synthesize or retain high concentrations of glycerol to maintain their osmotic balance (Blomberg, 2022; de Nadal and Posas, 2022; Hohmann, 2002). Intracellular glycerol concentration is partially regulated by Fps1, an aquaglyceroporin on the plasma membrane. Fps1 closes when extracellular osmolarity is high and opens when it is low, to expel glycerol and prevent cell rupture (Luyten *et al.*, 1995; Beese *et al.*, 2009; Lee *et al.*, 2013; Muir *et al.*, 2015; Ahmadpour *et al.*, 2016). The growth of the *fps1*Δ mutant was sensitive at 25 MPa (Figure 8A). The addition of 1 M sorbitol to the medium restored the growth of the *fps1*Δ mutant to the wild-type level, at 25 MPa (Figure 8A). Disruption of the glycerol synthase genes *GPP1* or *GPD1* increased, albeit partially, the high-pressure growth ability of the *fps1*Δ mutant (Figure 8B). Furthermore, single deletion of *GPP1* enhanced high-pressure growth in the wild-type strain, although deletion of other glycerol biosynthetic genes had no promotive effect (Figure 8B).

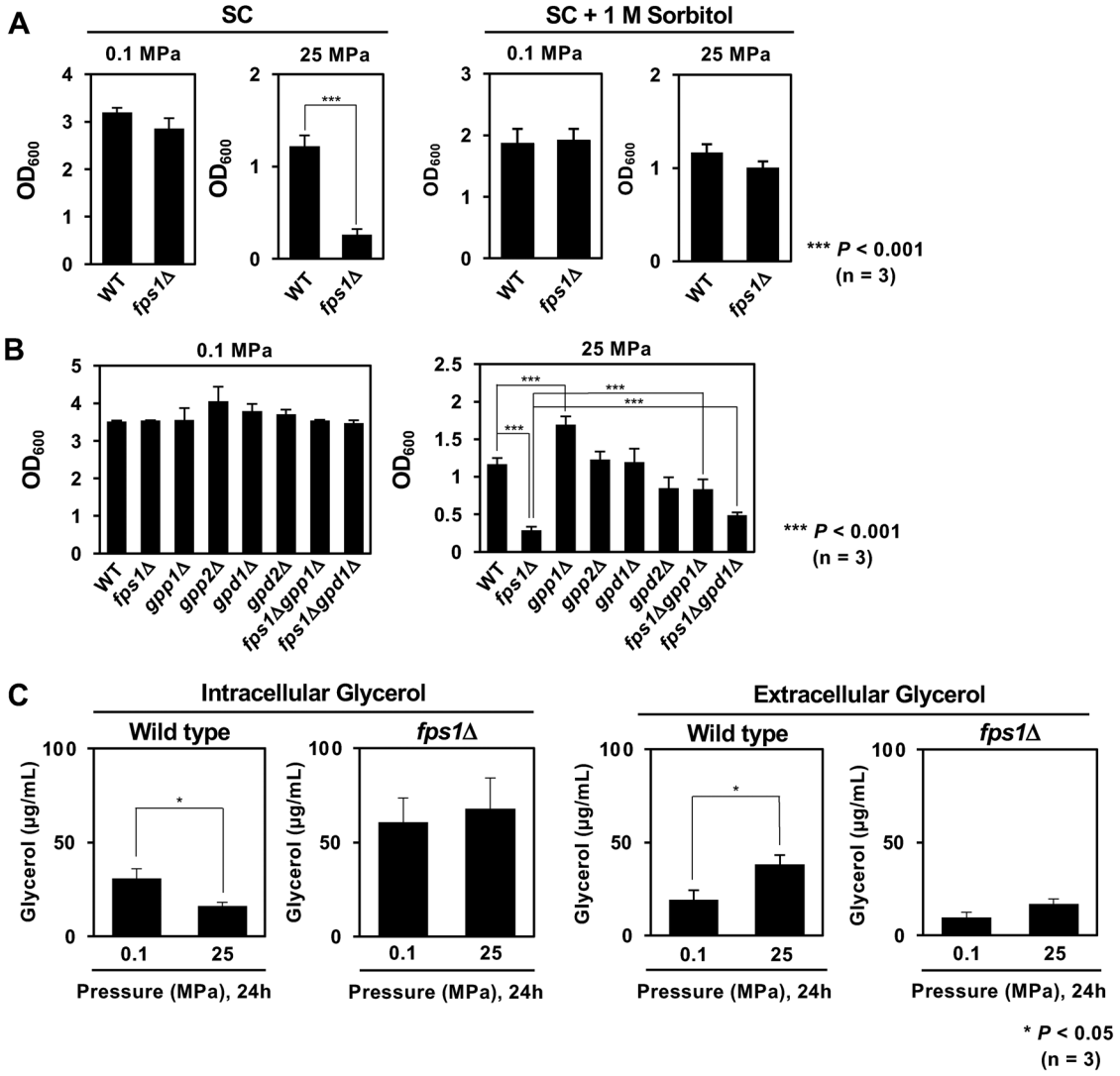

FIGURE 8: Glycerol efflux via Aquaglyceroporin Fps1 is required for high-pressure growth. (A) Wild-type and *fps1*Δ cells were cultured in SC medium with or without 1-M sorbitol at 0.1 or 25 MPa. (B) Mutants defective in glycerol synthesis were cultured in SC medium at 0.1 or 25 MPa. (C) Measurement of intracellular and extracellular glycerol levels after incubating cells at 0.1 or 25 MPa for 24 h with an initial OD_{600} = 0.1. Glycerol levels were quantified using a glycerol assay kit. Data are presented as mean ± SD of three independent experiments.

Next, we analyzed the intracellular and extracellular glycerol concentrations. Wild-type and *fps1*Δ cells in SC medium were incubated at 0.1 MPa and 25 MPa for 24 h, starting with an initial OD_{600} of 0.1. Upon analyzing these cells, we found that the intracellular glycerol concentration in wild-type cells decreased markedly after high-pressure culture, whereas more glycerol accumulated extracellularly (Figure 8C). By contrast, *fps1*Δ cells had a threefold-higher intracellular glycerol concentration than wild-type cells, which remained unchanged even after high-pressure culture (Figure 8C). Thus, we concluded that wild-type cells expelled glycerol via Fps1 to cope with the high-pressure-induced excess water influx.

Furthermore, the ultrastructure of cells via transmission electron microscopy (TEM) showed that wild-type cells underwent no significant changes in cell morphology or cell-wall structure after incubation at 25 MPa (Figure 9). The ultrastructure of *fps1*Δ cells also appeared normal at 0.1 MPa. Notably, 20–40% of *fps1*Δ cells had sharply ruptured cell walls, without any abnormalities in their intracellular structures at 25 MPa (Figure 9, arrows). The *fps1*Δ cell wall is weakened by increased turgor pressure due to glycerol accumulation; high pressure might also have caused further damage to the cell wall, leading to cell rupture. To investigate cell-wall rupture in *fps1*Δ cell populations cultured at 25 MPa, as shown in Figure 9A, we visualized the cell wall using CFW staining and quantified dead cells using propidium iodide (PI) staining. Despite imaging under the same confocal laser microscopy settings, the cell walls of *fps1*Δ cells cultured at 25 MPa exhibited significantly stronger CFW staining than those of the wild-type cells (Figure 9B). However, we did not observe any cell-wall rupture visualized by CFW staining. Thus, it is conceivable that if the cell-wall ruptures during high-pressure culture, the cell contents may leak out, and the cells may exist as remnants that cannot maintain their cellular morphology and are not even stained by PI (Figure 9B, arrows).

Fps1 opening is likely regulated by Slt2 during high-pressure cultures

The upstream regulators of Fps1 were analyzed to determine the mechanism by which cells regulate Fps1 in response to high

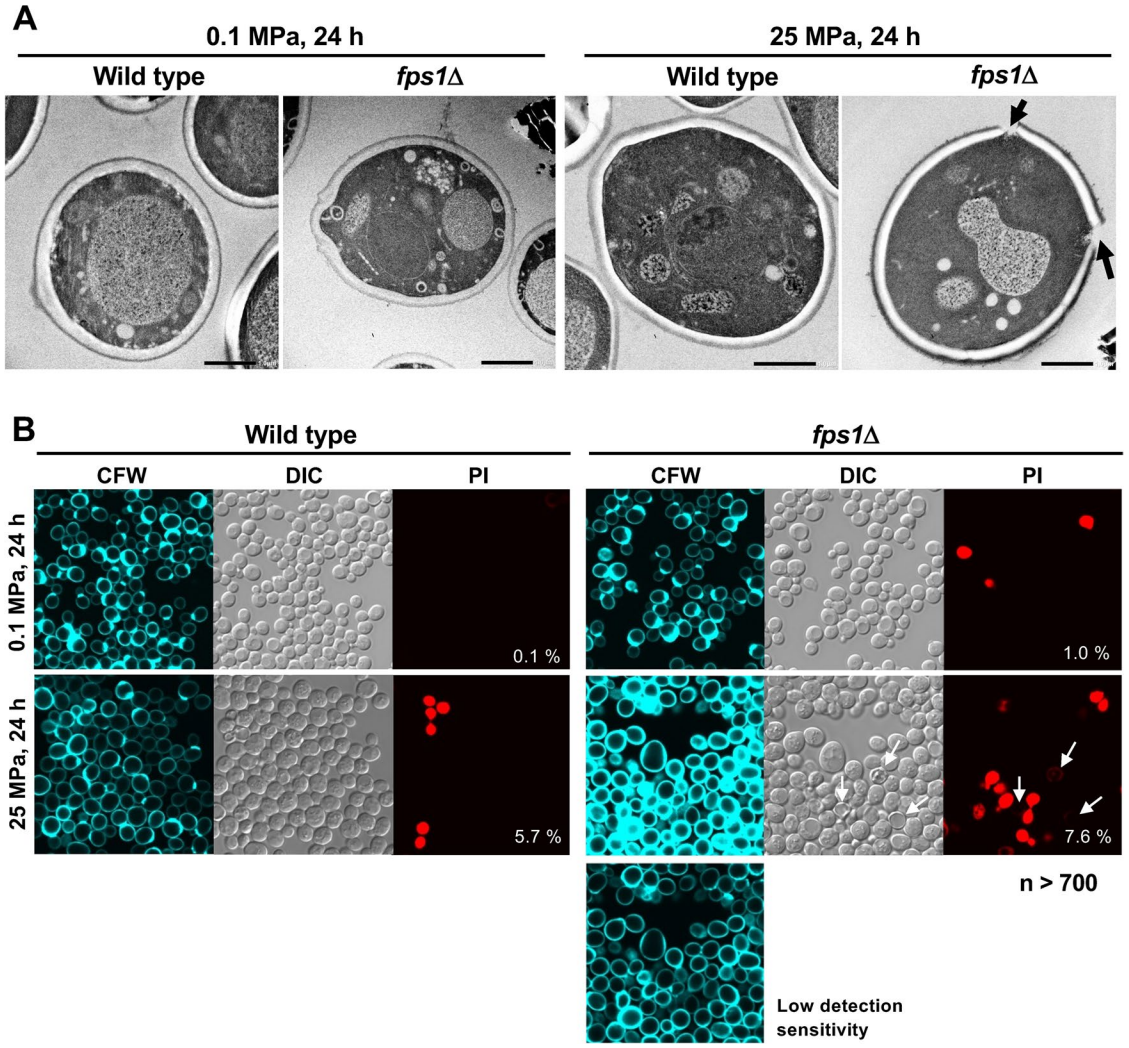

FIGURE 9: Ultrastructure of the cells observed using TEM. (A) Wild-type and *fps1*Δ cells were cultured at 0.1 or 25 MPa for 24 h, and after depressurization, the cells were subjected to rapid freezing using the sandwich method. In *fps1*Δ cells, the points of cell-wall breakage are indicated by arrows. Scale bars, 1.0 μm. (B) Wild-type and *fps1*Δ cells were cultured at 0.1 or 25 MPa for 24 h; after depressurization, the cells were stained with CFW and PI. The percentage of dead cells positive for PI staining is indicated (n > 700 for each strain). The arrows indicate remnants of dead cells, which are negative for PI staining.

pressure. Previous studies have indicated that Hog1 is a negative regulator of Fps1 opening, whereas Ypk1 and Slt2 are positive regulators (Figure 1) (Lee *et al.*, 2013; Muir *et al.*, 2015; Ahmadpour *et al.*, 2016). To determine which kinases are involved in the regulation of the Fps1 in response to high pressure, we examined the high-pressure growth ability of the *fps1*Δ mutant expressing Fps1-T231A (Hog1 target site; Thorsen *et al.*, 2006) or S537A (facilitates binding with Slt2; Ahmadpour *et al.*, 2016) at 25 MPa. We found that the Fps1-S537A strain showed high sensitivity, whereas the Fps1-T231A strain, as well as the wild-type strain, grew at 25 MPa (Figure 10A). We examined the phosphorylation of Fps1 using Western blotting and observed a high-molecular weight band of Fps1-3HA, the intensity of which increased slightly (2.2 ± 0.3 fold, $n = 3$) with increasing pressure at 25 MPa (Figure 10B). As expected, the high-molecular weight band of Fps1-3HA disappeared in cells expressing Fps1-S537A (Figure 10B). Phosphorylation of the S537 residue of Fps1 is essential for its interaction with Slt2; however, there is no evidence of its direct phosphorylation by Slt2 (Ahmadpour *et al.*, 2016).

The *slt2*Δ mutant was particularly sensitive to high pressure (Figures 4C and 10C), which was completely rescued by the addition of 1M sorbitol (Figure 10C). Therefore, the high-pressure sensitivity of the *slt2*Δ mutant was attributed to the excess water influx, at least in part, owing to its inability to open Fps1 and expel glycerol. The *hog1*Δ mutant also showed high-pressure sensitivity although the Fps1-T231A mutant grew at 25 MPa (Figure 10C). The result suggests Hog1 plays a role other than the Fps1 regulation under high pressure. The addition of 1M sorbitol did not restore high-pressure growth ability of the *hog1*Δ, *swi4*Δ, and *swi6*Δ mutants (Figure 10C). Notably, phosphorylation of Slt2 was also increased when cultured with 1 M sorbitol at 25 MPa where there is no excessive influx of water into cells (Figure 10D). These results suggest that the activation of the CWI pathway by high pressure may be due to the direct pressure effects on Wsc1 or the component proteins of the pathway, as well as activation via cell swelling caused by excess water influx under high pressure.

To verify whether the high-pressure sensitivity of the *slt2*Δ mutant was due to reduced Fps1 activity, we expressed $Fps1^{S537E}$, a

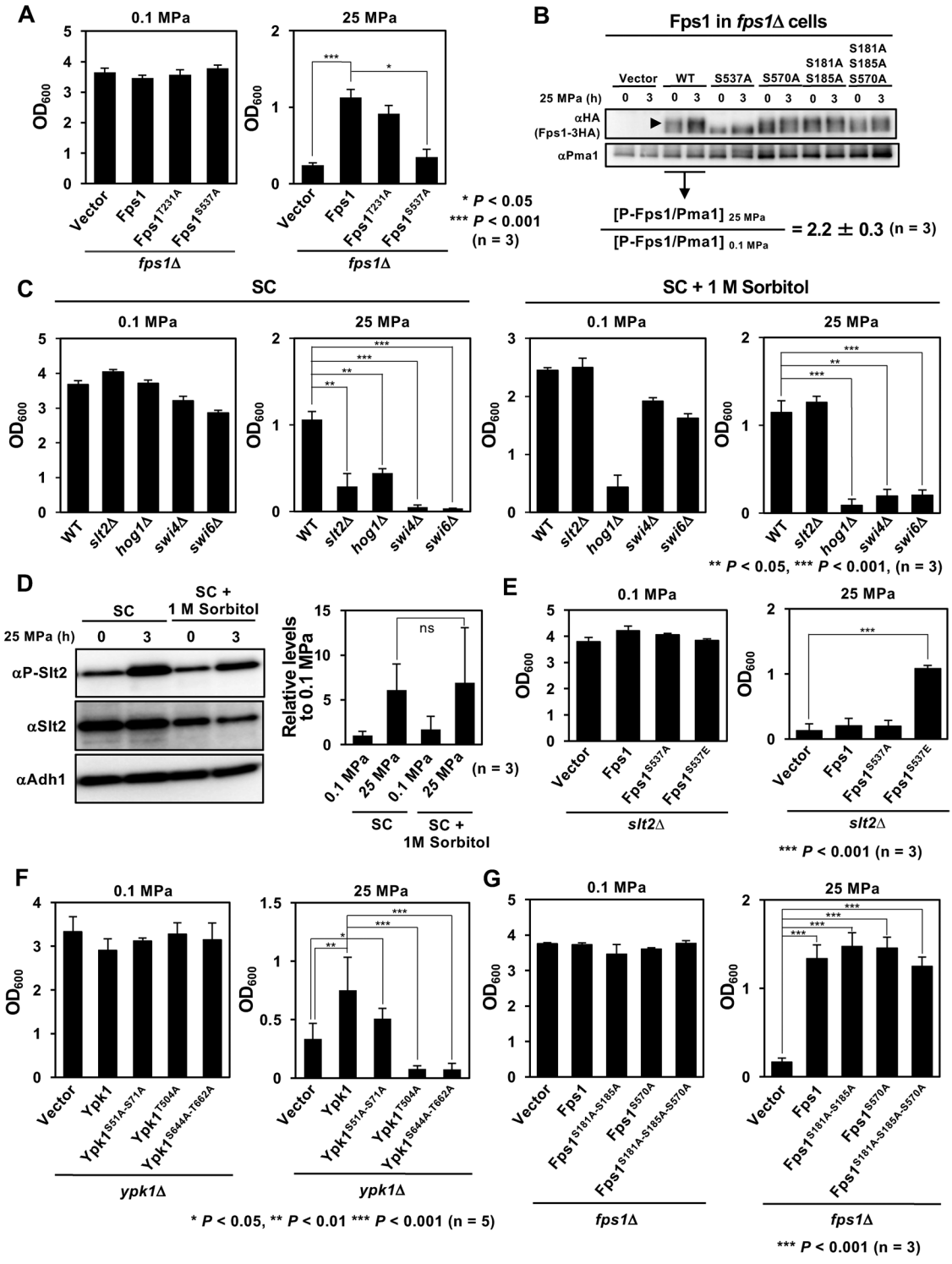

FIGURE 10: Slt2-dependent phosphorylation of Fps1 is required for growth under high pressure. (A) The Fps1 phosphorylation-site mutants were cultured in SC medium at 0.1 or 25 MPa. (B) Electrophoretic mobility of Fps1-3HA and its mutant forms was analyzed using Western blotting. Cells were cultured at 0.1 or 25 MPa for 3 h, and whole cell extracts were prepared. The arrowhead indicates a higher-molecular weight band of phospho-Fps1 (P-Fps1). The relative intensities, P-Fps1/Pma1 at 0.1 and 25 MPa, were quantified in an ImageQuant LAS4000 mini. (C) Wild-type, *slt2*Δ, *hog1*Δ, *swi4*Δ, and *swi6*Δ cells were cultured in SC medium with or without 1 M sorbitol at 0.1 or 25 MPa. (D) Wild-type cells were cultured in SC medium with or without 1-M sorbitol at 0.1 or 25 MPa for 3 h. Western blotting was performed as in Figure 4D. (E) *slt2*Δ cells expressing Fps1, Fps1^{S537A} or Fps1^{S537E} were cultured in SC medium at 0.1 or 25 MPa. (F) The Ypk1 phosphorylation-site mutants were cultured in SC medium at 0.1 or 25 MPa. (G) The Fps1 phosphorylation-site mutants were cultured in SC medium at 0.1 or 25 MPa. Data are presented as mean ± SD of three independent experiments.

simulated phosphorylated form of Fps1 at the S537 residue and found that it efficiently rescued the high-pressure sensitivity of the *slt2*Δ mutant (Figure 10E). Therefore, Slt2 activates Fps1, thereby preventing water influx and allowing cell growth under high pressure.

Ypk1 is required for growth under high pressure, independent of the regulation of Fps1

Fps1 is also phosphorylated by Ypk1 for its activation, depending on TORC2 signaling (Muir *et al.*, 2015). We found that the disruption of *YPK1* caused a severe defect in cell growth at 25 MPa, demonstrating the importance of Ypk1 (Figure 10F). Ypk1 is phosphorylated by multiple protein kinases such as Fpk1/Fpk2 (Rispal *et al.*, 2015), Pkh1/Pkh2 (Roelants *et al.*, 2002; Roelants *et al.*, 2004; Roelants *et al.*, 2010), and TORC2 (Roelants *et al.*, 2004; Muir *et al.*, 2015; Leskoske *et al.*, 2017; Figure 1). To infer which kinases are required for high-pressure growth via phosphorylation of Ypk1, we examined the effect of alanine substitutions for S51/S71 residues (Fpk1/Fpk2 target sites for Ypk1 inactivation; Roelants *et al.*, 2010), T504 residue (Pkh1/Pkh2 target site for Ypk1 activation; Roelants *et al.*, 2010), and S644/T662 residues (TORC2 target sites for Ypk1 activation; Roelants *et al.*, 2004; Roelants *et al.*, 2011) on cell growth under high pressure (Figure 1). While cells expressing Ypk1-S51A-S71A grew as efficiently as wild-type cells at 25 MPa, those expressing Ypk1-T504A or S644A-T662A showed severe growth defects under the pressure (Figure 10F). Thus, Ypk1 is likely phosphorylated by Pkh1/Pkh1 and TORC2 following high pressure. As shown in Figure 6, cells swelled after high-pressure incubation, and the eisosome structure disappeared. This raises the possibility that Slm1, localized in the eisosome, is released by high pressure and eventually binds to and activates TORC2, ultimately phosphorylating Ypk1 (Figure 1; Berchtold *et al.*, 2012; Riggi *et al.*, 2018). To test this hypothesis in our preliminary experiments, Lsp1-mCherry/Slm1-GFP-coexpressing and Avo3-3 × mCherry/Slm1-GFP-coexpressing strains were constructed, and any alterations in the colocalization of each strain under high pressure were observed using confocal laser microscopy. Avo3 and Lsp1 are components of TORC2 and the eisosome, respectively (Eltschinger and Loewith, 2016; Babst, 2019). We found that the colocalization of Lsp1-mCherry and Slm1-GFP decreased after cell incubation at 25 MPa, whereas that of Avo3-3 × mCherry and Slm1-GFP appeared to increase, suggesting TORC2 activation (Supplemental Figure S1A). Furthermore, phospho-Ypk1 was detected using a rabbit monoclonal antibody for phospho-PKC (pan) (zeta Thr410) (190D10), which reacts with the phosphorylated T504 residue (Niles *et al.*, 2012), and after incubation at 25 MPa for 3 h, its phosphorylation level increased sevenfold. (Supplemental Figure S1B).

To test whether phosphorylation of Fps1 by Ypk1 is required for high-pressure growth, the effect of phosphorylation site mutations was examined. Residue S570 of Fps1 is majorly phosphorylated by Ypk1, while the phosphorylation of residues S181 and S185 has also been reported (Figure 1; Muir *et al.*, 2015). Both the Fps1-S570A-substituted and S181A-S185A-S570A triple-substituted strains grew as well as the wild-type strain (Figure 10G). Consistent with this result, the electrophoretic mobility of the alanine substitution mutants Fps1-S570A-3HA, Fps1-A181A-S185A-3HA, and Fps1-A181A-S185A-S570A-3HA remained unaffected (Figure 10B). Thus, Ypk1 is unlikely to phosphorylate Fps1 in response to high pressure.

DISCUSSION

Based on the coincidental observation that cells moderately swell under high pressure, the importance of glycerol efflux by Fps1 and its regulation via the CWI pathway has been the focus of this study. We propose the presence of high-pressure signaling systems mediated by the stress sensor Wsc1 (Figure 11). In our model, high pressure activates the CWI pathway in two distinct modes. First, high pressure promotes water influx into yeast cells, thereby increasing turgor pressure, which in turn expands the cell walls and activates Wsc1 (Figures 3–6). Second, high pressure directly activates Wsc1 or influences the components within the CWI pathway, including Rom2, Rho1, or downstream kinases, as evidenced by our finding that phosphorylation of Slt2 was increased at 25 MPa even in the absence of cell swelling in 1 M sorbitol medium (Figure 10D). From the first perspective, the water influx caused by increased hydrostatic pressure is similar to that of hypoosmotic stress. In growing yeast cells, turgor pressure is estimated to be 0.5–1.5 MPa due to the influx of water driven by the osmotic gradient (Schaber *et al.*, 2010; Minc *et al.*, 2014; Atilgan *et al.*, 2015; Mishra *et al.*, 2022). The turgor pushes the cell membrane, further expanding the cell wall. Using an osmometer, we found the osmotic pressure of the SC medium to be 255 ± 0 mOsm/kg (n = 3), which corresponds to 0.588 MPa (nearly 0.6 MPa). Assuming that the turgor pressure of the cells was 1.0 MPa, the intracellular osmotic pressure was 1.6 MPa. Applying hydrostatic pressure to the cell culture caused a water influx into the cells until the water potentials inside and outside the cell became equivalent. Conversely, from the second perspective, it is conceivable that the high pressure of 25 MPa directly influences the structure of Wsc1, facilitates physical interactions between Wsc1 and Rom2, or even modifies the phosphorylating activity of kinases within the CWI pathway. However, no definitive conclusions have been reached regarding pressure-induced structural changes in Wsc1, the enhanced interaction between Wsc1 and Rom2, or any modifications to the kinase activities under high pressure.

High pressure may also cause some perturbation to the cell wall, as suggested by our observations that cells remain swollen at least 15 min post depressurization (Figure 6). However, there is currently no direct evidence demonstrating that high pressures of 25 MPa damage cell walls. Because high hydrostatic pressure has little effect on covalent binding (Chen *et al.*, 2017), it is unlikely that the β1, 3-glucan or β1,6-glucan networks are cleaved by high pressure. Rather, we suspect that high pressure may have a greater effect on the levels of cell-wall mannoproteins. Our previous DNA microarray results showed that transcription of the gene encoding for the major cell-wall mannoprotein Cwp1 was markedly reduced under 25 MPa; instead, the *DAN/TIR* family mannoprotein genes, which are typically induced under hypoxic conditions (Abramova *et al.*, 2001), were significantly enhanced (Abe, 2007). Although their protein levels have not been examined, the composition of mannoproteins may change with high pressure, and eventually, cell-wall elasticity may change. Once the CWI pathway is activated, Slt2 kinase promotes glycerol efflux through aquaglyceroporin Fps1, thereby allowing for cells to expel glycerol and adjust the osmotic pressure balance across the plasma membrane (Figure 8). Under high pressure, the high molecular weight band of Fps1 increased, suggesting enhanced Fps1 phosphorylation (Figure 10B). However, a similar high molecular weight band of Fps1 was also observed in the *slt2*Δ mutant, although it disappeared in Fps1^{S537A} (our unpublished observation). This suggests other kinases besides Slt2 that phosphorylate Fps1 at the S537 residue. Because phosphorylation of Fps1-S537 residue is critical for binding to Slt2, there may be other sites of authentic phosphorylation by Slt2. The role of Slt2 in growth under high pressure extends beyond the activation of Fps1. It also involves the phosphorylation of Swi4/Swi6 and the subsequent transcriptional induction of numerous downstream genes. The validity

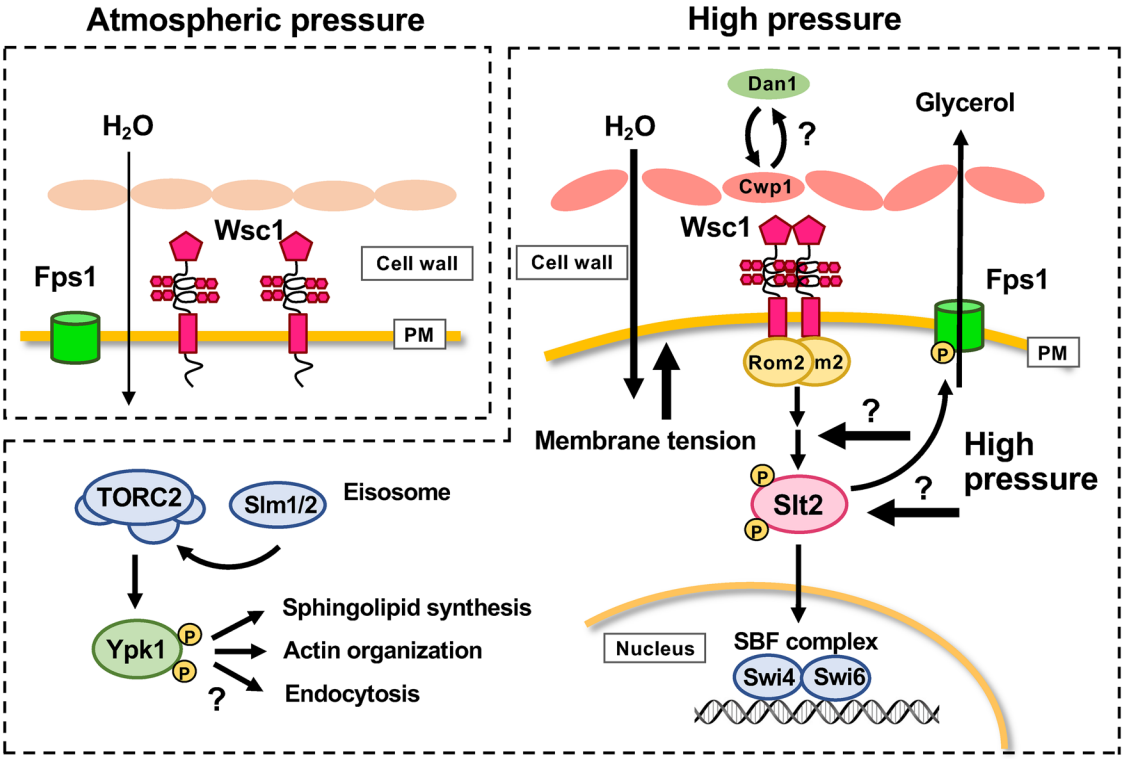

FIGURE 11: Model illustrating the activation of the CWI pathway by high hydrostatic pressure. The application of pressure to the cell leads to an excessive influx of water. The perturbation of the cell wall due to high pressure results in further water influx, increasing the risk of cell rupture. To prevent this, Wsc1 detects cell-wall stretching and activates the CWI pathway. High pressure may also affect proteins involved in the CWI pathway. Once the CWI pathway is activated, Slt2 kinase phosphorylates the aquaglyceroporin Fps1. Phosphorylated Fps1 facilitates its opening, enabling the cells to release glycerol and restore the osmotic pressure balance across the plasma membrane. Slt2 also regulates the nuclear translocation of Swi4/Swi6 in response to high pressure for activation of unidentified gene transcription. The TORC2-Ypk1 pathway operates independently of Fps1 regulation under high pressure.

of this assertion is supported by the significant high-pressure sensitivity observed upon the loss of *SWI4* or *SWI6*, as well as the translocation of Swi4 and Swi6 to the nucleus in response to high pressure. (Figure 5).

As per the TEM images of *fps1*Δ cells, the cell wall ruptured sharply after a high-pressure incubation (Figure 9A). This observation may be due to the localized weakening of the cell wall by increased turgor pressure due to glycerol accumulation in the *fps1*Δ cells. High pressure may have caused further damage to the cell wall in the *fps1*Δ mutant, leading to cell rupture. However, we cannot rule out the possibility that the weakened *fps1*Δ cell walls were ruptured during TEM sample preparation by the sandwich freezing method (Yamaguchi *et al.*, 2021a; Yamaguchi *et al.*, 2021b). It is unclear why the cell wall of the *fps1*Δ mutant was strongly stained with CFW following high-pressure incubation compared with that of the wild-type strain (Figure 9B). It is possible that the cell wall became more relaxed and thus more readily bound to CFW, or that the chitin content of the cell wall increased when the *fps1*Δ mutant was cultured under high pressure.

Although this study showed the importance of Ypk1 kinase in high-pressure growth (Figure 10F), it did not provide evidence that Ypk1 regulates the opening of Fps1 by phosphorylation (Figure 10G). Rather, alanine substitutions at Ypk1 residues, phosphorylated by TORC2 and Pkh1/Pkh2 kinases, prevented high-pressure growth (Figure 10F). TORC2-Ypk1 regulates polarization of the actin cytoskeleton and sphingolipid biosynthesis (Kamada *et al.*, 2005; Tabuchi *et al.*, 2006; Roelants *et al.*, 2011; Rispal *et al.*, 2015). Therefore, the regulation of sphingolipid synthesis or actin organization may be important for high-pressure adaptation. Indeed, high pressures stiffen membrane lipid bilayers (Winter, 2002; Matsuki *et al.*, 2013), which may adversely affect membrane protein functions, membrane fusion, or membrane trafficking. Furthermore, hypoosmotic stress causes the depolymerization of the actin cytoskeleton (Gualtieri *et al.*, 2004). To cope with these pleiotropic effects of high pressure, yeast cells may activate Fps1 via the CWI pathway to expel glycerol and avoid cell rupture, promote sphingolipid synthesis via the TORC2-Ypk1 pathway to maintain membrane homeostasis, and regulate actin cytoskeleton organization. Therefore, the regulation of sphingolipid synthesis and actin cytoskeleton via the TORC2-Ypk1 pathway is an interesting research target for understanding the physiological responses to high hydrostatic pressure in yeast.

Our previous studies have shown that defects in *TRP1*, *TAT2*, TORC1-EGOC, or poorly characterized genes such as *EHG1/MAY24* cause severe high-pressure sensitivity (Abe and Horikoshi, 2000; Abe and Minegishi, 2008; Kurosaka *et al.*, 2019; Uemura *et al.*, 2020). On the contrary, the defects in the CWI pathway and Fps1 shown in this study caused relatively mild sensitivity to high-pressure. This is probably because the former defects cause impaired nutrient uptake or aberrant glutamine accumulation under 25 MPa, resulting in rapid growth arrest after pressurization, whereas the latter defects are due to an inability to prevent water influx under high pressure, which causes the negative effects on growth to progress slowly. Yeasts possess two types of aquaporins, Aqy1 and Aqy2. However, both alleles are nonfunctional in experimental strains

derived from S288C, such as strain BY4742 (Sabir *et al.*, 2017). Therefore, the water influx into the cell when exposed to hypoosmotic or high hydrostatic pressure stress is thought to be mainly due to passive diffusion across the plasma membrane lipid bilayers. Passive diffusion of water across the lipid bilayer is much slower than water flux through aquaporins. This could explain why the effects of high-pressure stress are relatively mild. The Σ1278b strain and the naturally occurring *S. cerevisiae* strains have functional *AQY* alleles (Laize *et al.*, 1999). Therefore, the effects of hypoosmotic and high-pressure stress in these strains could be more severe than in the experimental strains. The osmotic pressure of the SC medium was 255 mOsm/kg, which corresponds to 127.5 mM NaCl. When it rains, the ambient osmotic pressure drops to near zero, exposing naturally occurring yeasts to greater hypoosmotic stress. Exposure to high hydrostatic pressure under such low osmotic pressure would pose a threat to their survival.

Meanwhile, the ambient osmotic pressure is isotonic for human and other animal cells. Therefore, excessive water influx due to high-water-pressure loading, as observed in yeast in this study, would not occur. However, when human endothelial cells are subjected to a pressure of 50 mm Hg (~6.7 kPa), which corresponds to a transient increase in blood pressure during exercise, water is extruded from the cell via aquaporin 1, causing cell contraction and plasma membrane deformation (Yoshino *et al.*, 2020). Consequently, Pkc1 is activated via the G protein-coupled receptor and phospholipase C, which in turn activates the Ras/ERK pathway, ultimately leading to the formation of complex tubular vascular structures (Yoshino *et al.*, 2020). Because aquaporins are channels, if the water potential is equivalent inside and outside the cells, no water efflux should occur even when the pressure is 50 mm Hg. However, because the pressure is very weak, the pressure applied at different sites in a single cell may be different, and water may be extruded through aquaporins at lower-pressure sites.

The effects of high hydrostatic pressure are influenced not only by the magnitude of the applied pressure but also by the duration of the pressurization. As a result, the impact on the complex metabolic processes of living cell systems cannot be generalized. To gain a comprehensive understanding of the effects of pressure, it is necessary to employ the extensive knowledge of yeast cell biology and sophisticated molecular genetic tools in advanced transcriptomics, proteomics, and metabolomics studies. These findings have the potential to be translated to mammalian cells and contribute to enhancing cellular health under both normal and stress conditions.

MATERIALS AND METHODS

Request a protocol through *Bio-protocol*.

Yeast strains and media

The parental wild-type strain BY4742 and the deletion mutants used in this study are listed in Table 1. Strains DL376 (*pkc1*Δ) and DL100 (the parental strain of DL376) were kindly provided by Dr. David Levin of Boston University Goldman School of Dental Medicine through Dr. Hidetoshi Iida of Tokyo Gakugei University (Levin and Bartlett-Heubusch, 1992). The two strains were transformed with YCplac22 (*TRP1, CEN*) to provide tryptophan prototrophy. Cells were grown in SC medium or YPD medium at 25°C under 0.1 MPa or 25 MPa (Abe and Minegishi, 2008). The SC medium contained 0.67% yeast nitrogen base without amino acids (Becton, Dickinson and Company, MD), 2% D-glucose, 20 μg/mL methionine, 90 μg/mL leucine, 30 μg/mL isoleucine, 40 μg/mL tryptophan, 20 μg/mL histidine, 30 μg/mL lysine, 20 μg/mL methionine, 50 μg/mL phenylalanine, 30 μg/mL tyrosine, 20 μg/mL arginine, 100 μg/mL aspartic acid, 100 μg/mL glutamic acid, 400 μg/mL serine, and 200 μg/mL threonine. YPD medium contains 1% Bacto yeast extract (Becton, Dickinson and Company), 2% Bacto peptone (Becton, Dickinson and Company), and 2% D-glucose.

High-pressure cell culture

For most experiments examining growth efficiency under high pressure, growing cells in shaking culture were diluted in SC or YPD medium to an OD_{600} of 0.01 (Figure 2). The diluted cells were transferred to sterile 1.8-mL tubes and sealed with Parafilm (Bemis Corp., Neenah, WI). The tubes were placed in a 500-mL high-pressure chamber (Abe and Minegishi, 2008) and subjected to 25 MPa at 25°C for 48 h. After depressurization, cell growth was evaluated by measuring OD_{600} using a PD-303 spectrophotometer (Apel, Kawaguchi, Japan). Here, $OD_{600} = 1.0$ corresponds to 1.65×10^7 cells/mL in our device setup.

Generation of plasmids and mutant strains

The plasmids used in the present study are listed in Table 2. Polymerase chain reaction (PCR)-based site-directed mutagenesis was performed using the appropriate primers. The primer sequences will be disclosed upon reasonable request. Homologous recombination, using pJT6 (GFP, *HIS3*) and pJT601 (mCherry, *URA3*), was used to tag genes in the yeast genome with GFP and mCherry, respectively (kind gifts from Dr. Jiro Toshima of Tokyo University of Science, (Kawada *et al.*, 2015). Plasmids encoding HA-Rho1 (SP333; *LEU2, CEN*), HA-Rho1^{F35L} (SP335; *LEU2, CEN*), and HA-Rho1^{Q68H} (SP336; *LEU2, CEN*) were kindly provided by Dr. Satoshi Yoshida of Waseda University (Yoshida *et al.*, 2009). pBSK-*SFK1*-3 × mCherry-*CaURA3* was kindly provided by Dr. Takuma Kishimoto of Hokkaido University Graduate School of Life Science (Kishimoto *et al.*, 2021). To generate Avo3-3 × mCherry strain, a DNA fragment encoding a *C*-terminal domain of Avo3 was amplified by PCR and was inserted into pBSK-*SFK1*-3 × mCherry-*CaURA3* of which *SFK1* gene had been removed. The resulting plasmid was linearized by digestion with *Eco*RV and introduced into the wild-type strain harboring *SLM1*-GFP in the genome.

Western blotting

Whole-cell extract preparation was performed as previously described (Ishii *et al.*, 2022). Briefly, 1.65×10^8 cells were collected by centrifugation; serially washed with 10 mM NaN_3, 10 mM NaF, and lysis buffer A (50-mM Tris-HCl, 5-mM EDTA, 10-mM NaN_3, and Complete EDTA-free tablet; Roche Diagnostics, Mannheim, Germany); disrupted with glass beads at 4°C. Unbroken cells and debris were removed by centrifugation at 900 × *g* for 5 min, and purified lysates were treated with 5% (wt/vol) SDS and 5% (vol/vol) 2-mercaptoethanol at 37°C for 10 min. Whole-cell extract preparation to detect phospho-Slt2 was performed as previously described (Wilk *et al.*, 2010) with some modifications. Yeast cells amounting to 5×10^7 in SC medium were treated with 255-mM NaOH–1% 2-mercaptoethanol on ice for 15 min, then 6% trichloroacetic acid (TCA) was added and cells were kept on ice for another 15 min. The cell pellet was collected after centrifugation at 15,000 × *g* for 5 min, washed with 1-M Tris-HCl (pH 6.8), and was treated with a sample buffer (65-mM Tris [pH6.8], 2% SDS, 10% glycerol, 100-mM DTT, 0.002% BPB) to denature proteins at 95°C for 5 min. The supernatant after centrifugation at 15,000 × *g* for 5 min was used for Western blotting. Whole-cell extract preparation to detect phospho-Ypk1 was performed as previously described (Roelants *et al.*, 2011) with some modifications. Yeast cells amounting to 1.65×10^7 were

Strains	Genotype	Source or reference
BY4742	*MATa his3Δ1 leu2Δ0 lys2Δ0 ura3Δ0*	Brachmann *et al.*, 1998
16672	*wsc1Δ::kanMX4* in BY4742	Winzeler *et al.*, 1999
11161	*wsc2Δ::kanMX4* in BY4742	Winzeler *et al.*, 1999
16255	*wsc3Δ::kanMX4* in BY4742	Winzeler *et al.*, 1999
15241	*mid2Δ::kanMX4* in BY4742	Winzeler *et al.*, 1999
14653	*mtl1Δ::kanMX4* in BY4742	Winzeler *et al.*, 1999
14700	*rom1Δ::kanMX4* in BY4742	Winzeler *et al.*, 1999
15280	*rom2Δ::kanMX4* in BY4742	Winzeler *et al.*, 1999
16152	*bem2Δ::kanMX4* in BY4742	Winzeler *et al.*, 1999
14225	*sac7Δ::kanMX4* in BY4742	Winzeler *et al.*, 1999
13937	*lrg1Δ::kanMX4* in BY4742	Winzeler *et al.*, 1999
12390	*bag7Δ::kanMX4* in BY4742	Winzeler *et al.*, 1999
DL100	*MATa his4 leu2-3,112 trp1-1 ura3-52 can1*	Siliciano and Tatchell, 1984
DL376	*pkc1Δ::Leu2* in DL100	Levin and Bartlett-Heubusch, 1992
11328	*bck1Δ::kanMX4* in BY4742	Winzeler *et al.*, 1999
12487	*mkk1Δ::kanMX4* in BY4742	Winzeler *et al.*, 1999
12112	*mkk2Δ::kanMX4* in BY4742	Winzeler *et al.*, 1999
10993	*slt2Δ::kanMX4* in BY4742	Winzeler *et al.*, 1999
TMY1482	*SWI4-GFP::HIS3* in BY4742	This study
TMC086	*SWI6-GFP::HIS3* in BY4742	This study
12739	*rlm1Δ::kanMX4* in BY4742	Winzeler *et al.*, 1999
16109	*swi4Δ::kanMX4* in BY4742	Winzeler *et al.*, 1999
14131	*swi6Δ::kanMX4* in BY4742	Winzeler *et al.*, 1999
AFY7	*PIL1*-mCherry::*URA3* in BY4742	Ishii *et al.*, 2022
MSY1	*NCE102*-mCherry::*URA3* in BY4742	This study
MSY17	*SUR7*-mCherry::*URA3* in BY4742	This study
11531	*fps1Δ::kanMX4* in BY4742	Winzeler *et al.*, 1999
11446	*gpp1Δ::kanMX4* in BY4742	Winzeler *et al.*, 1999
10199	*gpp2Δ::kanMX4* in BY4742	Winzeler *et al.*, 1999
13718	*gpd1Δ::kanMX4* in BY4742	Winzeler *et al.*, 1999
11751	*gpd2Δ::kanMX4* in BY4742	Winzeler *et al.*, 1999
TTY146	*fps1Δ::HphMX6 gpp1::kanMX4* in BY4742	This study
TTY147	*fps1Δ::HphMX6 gpd1::kanMX4* in BY4742	This study
TTY108	*SLM1-GFP::HIS3 LSP1-mCherry::URA3* in BY4742	This study
TTY113	*SLM1-GFP::HIS3 AVO3-3 × mCherry::URA3* in BY4742	This study
14976	*ypk1Δ::kanMX4* in BY4742	Winzeler *et al.*, 1999
TMC123	*NCE102*-mCherry::*URA3* in *wsc1Δ*	This study
TMC124	*NCE102*-mCherry::*URA3* in *slt2Δ*	This study
TMC125	*NCE102*-mCherry::*URA3* in *fps1Δ*	This study

TABLE 1: Strains used in this study.

collected by centrifugation at 6000 × *g* for 1 min. After removing the supernatant, the cell pellet was frozen in liquid nitrogen and was treated with 150 µl of 1.85 M NaOH–7.4% 2-mercaptoethanol for 15 min on ice. Then, 150 µl of 50% TCA was added to the cell suspension to precipitate proteins on ice for 10 min. After removing the supernatant, the proteins were washed twice with acetone and were denatured with the sample buffer at 95°C for 5 min. Proteins were separated by SDS–PAGE and transferred to Immobilon PVDF membranes (EMD Millipore, Billerica, MA). The membrane was incubated for 1 h with antibodies. The following antibodies were used: a monoclonal antibody for HA (Medical & Biological Laboratories, Nagoya, Japan), a rabbit polyclonal antibody for Adh1 (Rockland Immunochemicals, Gilbersville, PA), a rabbit polyclonal antibody for Pma1 (Usami *et al.*, 2014), a mouse monoclonal antibody for Slt2

Plasmid	Description	Source or reference
pUA35	3HA *URA3 CEN*4	Laboratory stock
pTM35	*GFP URA3 CEN*4	Laboratory stock
YCplac111	*LEU2 CEN4*	Gietz and Sugino, 1988
YEplac181	*LEU2 2 μ*	Gietz and Sugino, 1988
YCplac22	*TRP1 CEN4*	Gietz and Sugino, 1988
pRS313	*HIS3 CEN6*	Sikorski and Hieter, 1989
pRS426	*URA3 2 μ*	Sikorski and Hieter, 1989
pTAT1-GFP	*TAT1*-GFP driven by its own promoter in pRS313	This study
pMB1	*WSC1*-3HA driven by its own promoter in pUA35	This study
pMB20	*WSC1*-3HA-C27A-C49A-C53A-C69A-C71A-C86A-C90A-C98A driven by its own promoter in pUA35	This study
pMB21	*WSC1*-3HA-Δ111-250 driven by its own promoter in pUA35	This study
pMB22	*WSC1*-3HA-Δ22-250 driven by its own promoter in pUA35	This study
pMB74	*WSC1*-3HA-N344A-P345A-F346A driven by its own promoter in pUA35	This study
pMB23	*WSC1*-3HA-Y303A driven by its own promoter in pUA35	This study
pSS21	*WSC1*-GFP driven by its own promoter in pTM35	This study
pMB36	*WSC1*-GFP-C27A-C49A-C53A-C69A-C71A-C86A-C90A-C98A driven by its own promoter in pTM35	This study
pMB82	*WSC1*-GFP-Δ111-250 driven by its own promoter in pTM35	This study
pMB35	*WSC1*-GFP-Δ22-250 driven by its own promoter in pTM35	This study
pMB80	*WSC1*-GFP-N344A-P345A-F346A driven by its own promoter in pTM35	This study
pMB55	*SWI4*-3HA driven by its own promoter in pUA35	This study
pMB56	*SWI6*-3HA driven by its own promoter in pUA35	This study
pMB83	*RLM1*-3HA driven by its own promoter in pUA35	This study
pMB84	*RLM1*-3HA driven by its own promoter in pRS426	This study
pCZY1	UPRE-*lacZ URA3 2 μ*	Kawahara *et al.*, 1997
pMB49	*lacZ URA3 CEN4*	This study
pMB85	*lacZ* driven by *SLT2* promoter in pMB49	This study
pMB86	*lacZ* driven by *MLP1* promoter in pMB49	This study
pMB87	*lacZ* driven by *YIL117c* promoter in pMB49	This study
SP333	HA-*RHO1* driven by its own promoter *LEU2 CEN*	Yoshida *et al.*, 2009
SP335	HA-*RHO1*-F35L driven by its own promoter *LEU2 CEN*	Yoshida *et al.*, 2009
SP336	HA-*RHO1*-Q68H driven by its own promoter *LEU2 CEN*	Yoshida *et al.*, 2009
pME29	*PKC1* driven by its own promoter in YEplac181	This study
pME30	*PKC1*-R398P driven by its own promoter in YCplac111	This study
pTNK5	*FPS1* driven by its own promoter in pUA35	This study
pTNK8	*FPS1*-T231A driven by its own promoter in pUA35	This study
pTNK9	*FPS1*-S537A driven by its own promoter in pUA35	This study
pSS46	*FPS1*-S537E driven by its own promoter in pUA35	This study
pTNK10	*FPS1*-S570A driven by its own promoter in pUA35	This study
pTNK22	*FPS1*-S181A-S185A driven by its own promoter in pUA35	This study
pTNK23	*FPS1*-S181A-S185A-S570A driven by its own promoter in pUA35	This study
pSS10	*FPS1*-3HA driven by its own promoter in pUA35	This study
pSS26	*FPS1*-3HA-S537A driven by its own promoter in pUA35	This study
pSS12	*FPS1*-3HA-S570A driven by its own promoter in pUA35	This study

TABLE 2: Plasmids used in this study.

(*Continues*)

Plasmid	Description	Source or reference
pSS16	*FPS1*-3HA-S181A-S185A driven by its own promoter in pUA35	This study
pSS14	*FPS1*-3HA-S181A-S185A-S570A driven by its own promoter in pUA35	This study
pSS6	*YPK1* driven by its own promoter in pUA35	This study
pTNK11	*YPK1*-S51A-S71A driven by its own promoter in pUA35	This study
pTNK7	*YPK1*-T504A driven by its own promoter in pUA35	This study
pTNK14	*YPK1*-S644A-T662A driven by its own promoter in pUA35	This study
pTM102	pBSK (+) -*SFK1*-3 × mCherry	Kishimoto *et al.*, 2021
pJT6	GFP *HIS3*	Kawada *et al.*, 2015
pJT601	mCherry *URA3*	Kawada *et al.*, 2015

TABLE 2: Plasmids used in this study. Continued

(catalogue no. sc-133189, Santa Cruz Biotechnology, TX), a rabbit monoclonal antibody phospho-p44/42 MAPK (Erk1/2, Thr202/Tyr204; catalogue no. 4376, Cell Signaling Technology, MA) to detect phospho-Slt2, a rabbit polyclonal antibody for Ypk1 (a kind gift from Dr. Mitsuaki Tabuchi of Kagawa University; Ishino *et al.*, 2022), and a rabbit monoclonal antibody for phospho-PKC (pan) (zeta Thr410) (190D10) (catalogue no. 2060, Signaling Technology) to detect phospho-Ypk1 (Niles *et al.*, 2012). The membranes were washed and incubated for 30 min with horseradish peroxidase-conjugated goat anti-rabbit IgG (GE Healthcare Bio-Sciences, NJ). Labeling was performed using an enhanced chemiluminescence select kit (GE Healthcare Bio-Sciences). The chemiluminescence signals were detected in an ImageQuant LAS4000 mini (GE Healthcare Life Sciences, NJ)

lacZ reporter assay

Promoter regions from *SLT2* (nucleotides – 949 to 1), *MLP1* (nucleotides – 949 to 3), or *YIL117C* (nucleotides – 994 to 3) (Jung *et al.*, 2002) were amplified from genomic DNA of strain BY4742. Each DNA fragment was inserted into pMB49 (*lacZ, URA3, CEN4*), which was derived from pCZY (UPRE-*lacZ* reporter, *URA3, 2 μ*) by removing the UPRE region (Kawahara *et al.*, 1997). β-galactosidase assay was performed as described previously (Mochizuki *et al.*, 2015).

Cell staining with CFW and PI

Growing cells in SC medium were collected by centrifugation at 2400 × *g* for 10 s and resuspended with 50-mM Tris-HCl (pH 7.5) containing 1-μg/ml CFW (Fluorescence Brightener 28, MP Biomedicals, LLC, OH) and PI (LIVE/DEAD *Funga*Light Yeast Viability Kit, Life Technologies Corporation, OR) to stain the cell wall and dead cells, respectively.

Image collection and analyses on confocal laser microscope

Cells expressing GFP- or mCherry-tagged proteins were imaged using a confocal laser microscope (FV-3000) equipped with an objective lens UPLAPO60XOHR (NA 1.5) (Olympus, Tokyo, Japan). To determine the cell volume, cells were assumed to be spheres or ellipsoids. Using Tat1-GFP as a cell membrane marker (Ishii *et al.*, 2022), cross-sectional images of lt100 cells cultured under each condition were acquired. CellSens software (Olympus) was used to mark Tat1-GFP as a circle or ellipse, and the radius (*r* μm) or long (*a* μm) and short radii (*b* μm) were calculated. For spheres, the volume (μm^3) was approximated by $V = 4/3\pi * r^3$, and for ellipsoids, $V = 4/3\pi * a * b^2$. Changes in cell volume due to high-pressure incubation were measured by acquiring images at 0.1 MPa, immediately after depressurization. Colocalization of Lsp1-mCherry with Slm1-GFP or Avo3-3 × mCherry with Slm1-GFP was analyzed in mt50 cells from three independent experiments using cellSens software and represented by the Pearson colocalization coefficient.

Determination of glycerol concentration

Culture medium containing cells of 1.0 OD_{600} (1.65 × 10^7 cells) was centrifuged at 6000 × *g* for 1 min to separate the supernatant and cell pellet. The cell pellet was dissolved in 100 μl of sterilized deionized water and the mixture was heated at 95°C for 10 min. After cooling to room temperature, the mixture was centrifuged at 21,500 × *g* for 10 min to collect the supernatant. Glycerol concentrations in the samples were determined using a glycerol colorimetric assay kit (item no. 10010755, Cayman Chemical Company, MI) with an appropriate dilution.

Measurement of osmotic pressure

The osmotic pressure of SC medium was measured using a Fiske 210 osmometer (Advanced Instruments, MA).

TEM observation

Samples for TEM observation were prepared as described previously (Yamaguchi *et al.*, 2021a; Yamaguchi *et al.*, 2021b), with modifications. Cells cultured at 0.1 MPa or 25 MPa for 24 h in the SC medium were briefly centrifuged at 760 × *g* following depressurization, and less than 1 μl of the cell suspension was sandwiched between two copper disks (3 mm diameter) that had been prehydrophilized. The copper disks were then sandwiched between reverse-acting tweezers and dropped into a coolant for quick freezing. An isopentane: ethanol (4:1) mixture cooled with liquid nitrogen to a sherbet-like consistency (approximately – 130°C) was used as the coolant. The copper disks were immediately transferred to liquid nitrogen, cracked open, and then transferred to a fixing solution cooled with liquid nitrogen. Ethanol containing 2% glutaraldehyde and 1% tannic acid was used as a fixing solution. The samples in the fixing solution were kept at –80°C for 48 h, –20°C for 2 h, 4°C for 2 h, and finally returned to room temperature, in that order. Cells on copper disks were immersed in dehydrated ethanol for 30 min thrice and then overnight. Propylene oxide: resin (Agar low viscosity resin LV, catalogue no. R1078, Agar Scientific Ltd, Essex, UK) mixture was used for resin replacement of the samples, with the following mixing ratios in sequence; 1:0 (30 min, twice), 2:1 (1 h, once), 1:2 (1 h, once), 0:1 (overnight, once). The resin-substituted samples

were allowed to solidify for 24 h at 60°C. Ultrathin sections of 70 nm thickness were then prepared using an Ultracut E ultramicrotome (Reichert-Jung, Austria). The sections were stained with EM Stainer (catalogue no. 336, Nissin EM, Tokyo, Japan) for 30 min and lead stain (Sigma-Aldrich, MO) for 30 min. The samples were observed using a transmission electron microscope JEM-2100 (JEOL, Tokyo, Japan) equipped with a thermionic electron emission electron gun (LaB6 filament) at an acceleration voltage of 100 kV.

ACKNOWLEDGMENTS

We would like to thank Drs. Satoshi Yoshida, Jiro Toshima, Makoto Nagano, and Takuma Kishimoto for providing plasmids; Drs. David Levin and Hidetoshi Iida for providing yeast strains; Dr. Mitsuaki Tabuchi for providing the rabbit polyclonal antibody for Ypk1 and for his critical reading of this manuscript; Messrs. Katsuyuki Uematsu and Yosuke Ishihara for technical assistance on TEM sample preparations; and Drs. Wataru Nomura and Yoshiharu Inoue, and the laboratory members for facilitating valuable discussions. TEM observation was supported by the Center for Instrumental Analysis, College of Science and Engineering, Aoyama Gakuin University. This work was supported by a grant from the Japan Society for the Promotion of Science (No. 18K05397 and 22H02247 to F.A.) and a fund from Aoyama Gakuin University (Aoyama Vision 2019–2021) to F.A.

REFERENCES

Abe F, Minegishi H, Miura T, Nagahama T, Usami R, Horikoshi K (2006). Characterization of cold- and high-pressure-active polygalacturonases from a deep-sea yeast, *Cryptococcus liquefaciens* strain N6. Biosci Biotechnol Biochem 70, 296–299.

Abe F (2021). Molecular responses to high hydrostatic pressure in eukaryotes: Genetic insights from studies on *Saccharomyces cerevisiae*. Biology (Basel) 10, 1305.

Abe F (2007). Induction of *DAN/TIR* yeast cell wall mannoprotein genes in response to high hydrostatic pressure and low temperature. FEBS Lett 581, 4993–4998.

Abe F, Horikoshi K (2000). Tryptophan permease gene *TAT2* confers high-pressure growth in *Saccharomyces cerevisiae*. Mol Cell Biol 20, 8093–8102.

Abe F, Kato C, Horikoshi K (1999). Pressure-regulated metabolism in microorganisms. Trends Microbiol 7, 447–453.

Abe F, Minegishi H (2008). Global screening of genes essential for growth in high-pressure and cold environments: searching for basic adaptive strategies using a yeast deletion library. Genetics 178, 851–872.

Abramova NE, Cohen BD, Sertil O, Kapoor R, Davies KJ, Lowry CV (2001). Regulatory mechanisms controlling expression of the *DAN/TIR* mannoprotein genes during anaerobic remodeling of the cell wall in *Saccharomyces cerevisiae*. Genetics 157, 1169–1177.

Afoke NY, Byers PD, Hutton WC (1987). Contact pressures in the human hip joint. J Bone Joint Surg Br 69, 536–541.

Ahmadpour D, Maciaszczyk-Dziubinska E, Babazadeh R, Dahal S, Migocka M, Andersson M, Wysocki R, Tamas MJ, Hohmann S (2016). The mitogen-activated protein kinase Slt2 modulates arsenite transport through the aquaglyceroporin Fps1. FEBS Lett 590, 3649–3659.

Atilgan E, Magidson V, Khodjakov A, Chang F (2015). Morphogenesis of the fission yeast cell through cell wall expansion. Curr Biol 25, 2150–2157.

Babst M (2019). Eisosomes at the intersection of TORC1 and TORC2 regulation. Traffic 20, 543–551.

Banavar SP, Gomez C, Trogdon M, Petzold LR, Yi TM, Campas O (2018). Mechanical feedback coordinates cell wall expansion and assembly in yeast mating morphogenesis. PLoS Comput Biol 14, e1005940.

Bass D, Howe A, Brown N, Barton H, Demidova M, Michelle H, Li L, Sanders H, Watkinson SC, Willcock S, Richards TA (2007). Yeast forms dominate fungal diversity in the deep oceans. Proc Biol Sci 274, 3069–3077.

Beese SE, Negishi T, Levin DE (2009). Identification of positive regulators of the yeast fps1 glycerol channel. PLoS Genet 5, e1000738.

Berchtold D, Piccolis M, Chiaruttini N, Riezman I, Riezman H, Roux A, Walther TC, Loewith R (2012). Plasma membrane stress induces relocalization of Slm proteins and activation of TORC2 to promote sphingolipid synthesis. Nat Cell Biol 14, 542–547.

Bi E, Park HO (2012). Cell polarization and cytokinesis in budding yeast. Genetics 191, 347–387.

Blomberg A (2022). Yeast osmoregulation - glycerol still in pole position. FEMS Yeast Res 22, 1–20.

Bourges AC, Torres Montaguth OE, Ghosh A, Tadesse WM, Declerck N, Aertsen A, Royer CA (2017). High pressure activation of the *mrr* restriction endonuclease in *Escherichia coli* involves tetramer dissociation. Nucleic Acids Res 45, 5323–5332.

Brachmann CB, Davies A, Cost GJ, Caputo E, Li J, Hieter P, Boeke JD (1998). Designer deletion strains derived from *Saccharomyces cerevisiae* S288C: A useful set of strains and plasmids for PCR-mediated gene disruption and other applications. Yeast 14, 115–132.

Burgaud G, Hue NTM, Arzur D, Coton M, Perrier-Cornet J, Jebbar M, Barbier G (2015). Effects of hydrostatic pressure on yeasts isolated from deep-sea hydrothermal vents. Res Microbiol 166, 700–709.

Chen B, Hoffmann R, Cammi R (2017). The effect of pressure on organic reactions in fluids-a new theoretical perspective. Angew Chem Int Ed Engl 56, 11126–11142.

Cruz S, Munoz S, Manjon E, Garcia P, Sanchez Y (2013). The fission yeast cell wall stress sensor-like proteins Mtl2 and Wsc1 act by turning on the GTPase Rho1p but act independently of the cell wall integrity pathway. Microbiologyopen 2, 778–794.

Davi V, Chevalier L, Guo H, Tanimoto H, Barrett K, Couturier E, Boudaoud A, Minc N (2019). Systematic mapping of cell wall mechanics in the regulation of cell morphogenesis. Proc Natl Acad Sci USA 116, 13833–13838.

de Nadal E, Posas F (2022). The HOG pathway and the regulation of osmoadaptive responses in yeast. FEMS Yeast Res 22, 1–7.

Domitrovic T, Fernandes CM, Boy-Marcotte E, Kurtenbach E (2006). High hydrostatic pressure activates gene expression through Msn2/4 stress transcription factors which are involved in the acquired tolerance by mild pressure precondition in *Saccharomyces cerevisiae*. FEBS Lett 580, 6033–6038.

Douglas LM, Konopka JB (2014). Fungal membrane organization: the eisosome concept. Annu Rev Microbiol 68, 377–393.

Dupres V, Alsteens D, Wilk S, Hansen B, Heinisch JJ, Dufrene YF (2009). The yeast Wsc1 cell surface sensor behaves like a nanospring in vivo. Nat Chem Biol 5, 857–862.

Elhasi T, Blomberg A (2019). Integrins in disguise - mechanosensors in *Saccharomyces cerevisiae* as functional integrin analogues. Microb Cell 6, 335–355.

Eltschinger S, Loewith R (2016). TOR complexes and the maintenance of cellular homeostasis. Trends Cell Biol 26, 148–159.

Funada C, Tanino N, Fukaya M, Mikajiri Y, Nishiguchi M, Otake M, Nakasuji H, Kawahito R, Abe F (2022). *SOD1* mutations cause hypersensitivity to high-pressure-induced oxidative stress in *Saccharomyces cerevisiae*. Biochim Biophys Acta Gen Subj 1866, 130049.

Gietz RD, Sugino A (1988). New yeast-*Escherichia coli* shuttle vectors constructed with in vitro mutagenized yeast genes lacking six-base pair restriction sites. Gene 74, 527–534.

Gonzalez-Rubio G, Sastre-Vergara L, Molina M, Martin H, Fernandez-Acero T (2022). Substrates of the MAPK Slt2: Shaping yeast cell integrity. J Fungi (Basel) 8, 368.

Gualtieri T, Ragni E, Mizzi L, Fascio U, Popolo L (2004). The cell wall sensor Wsc1p is involved in reorganization of actin cytoskeleton in response to hypo-osmotic shock in *Saccharomyces cerevisiae*. Yeast 21, 1107–1120.

Heinisch JJ, Dupres V, Wilk S, Jendretzki A, Dufrene YF (2010). Single-molecule atomic force microscopy reveals clustering of the yeast plasma-membrane sensor Wsc1. PLoS One 5, e11104.

Hodder E, Guppy F, Covill D, Bush P (2020). The effect of hydrostatic pressure on proteoglycan production in articular cartilage in vitro: a meta-analysis. Osteoarthritis Cartilage 28, 1007–1019.

Hodge WA, Carlson KL, Fijan RS, Burgess RG, Riley PO, Harris WH, Mann RW (1989). Contact pressures from an instrumented hip endoprosthesis. J Bone Joint Surg Am 71, 1378–1386.

Hohmann S (2002). Osmotic stress signaling and osmoadaptation in yeasts. Microbiol Mol Biol Rev 66, 300–372.

Ishii R, Fukui A, Sakihama Y, Kitsukawa S, Futami A, Mochizuki T, Nagano M, Toshima J, Abe F (2022). Substrate-induced differential degradation and partitioning of the two tryptophan permeases Tat1 and Tat2 into eisosomes in *Saccharomyces cerevisiae*. Biochim Biophys Acta Biomembr 1864, 183858.

Ishino Y, Komatsu N, Sakata K, Yoshikawa D, Tani M, Maeda T, Morishige K, Yoshizawa K, Tanaka N, Tabuchi M (2022). Regulation of sphingolipid biosynthesis in the endoplasmic reticulum via signals from the plasma membrane in budding yeast. FEBS J 289, 457–472.

Iwahashi H (2015). Pressure-dependent gene activation in yeast cells. Subcell Biochem 72, 407–422.
Jimenez-Gutierrez E, Alegria-Carrasco E, Sellers-Moya A, Molina M, Martin H (2020). Not just the wall: the other ways to turn the yeast CWI pathway on. Int Microbiol 23, 107–119.
Jung US, Sobering AK, Romeo MJ, Levin DE (2002). Regulation of the yeast Rlm1 transcription factor by the Mpk1 cell wall integrity MAP kinase. Mol Microbiol 46, 781–789.
Kamada Y, Fujioka Y, Suzuki NN, Inagaki F, Wullschleger S, Loewith R, Hall MN, Ohsumi Y (2005). Tor2 directly phosphorylates the AGC kinase Ypk2 to regulate actin polarization. Mol Cell Biol 25, 7239–7248.
Kawada D, Kobayashi H, Tomita T, Nakata E, Nagano M, Siekhaus DE, Toshima JY, Toshima J (2015). The yeast arf-GAP Glo3p is required for the endocytic recycling of cell surface proteins. Biochim Biophys Acta 1853, 144–156.
Kawahara T, Yanagi H, Yura T, Mori K (1997). Endoplasmic reticulum stress-induced mRNA splicing permits synthesis of transcription factor Hac1p/Ern4p that activates the unfolded protein response. Mol Biol Cell 8, 1845–1862.
Kechagia JZ, Ivaska J, Roca-Cusachs P (2019). Integrins as biomechanical sensors of the microenvironment. Nat Rev Mol Cell Biol 20, 457–473.
Kim KY, Truman AW, Caesar S, Schlenstedt G, Levin DE (2010). Yeast Mpk1 cell wall integrity mitogen-activated protein kinase regulates nucleocytoplasmic shuttling of the Swi6 transcriptional regulator. Mol Biol Cell 21, 1609–1619.
Kishimoto T, Mioka T, Itoh E, Williams DE, Andersen RJ, Tanaka K (2021). Phospholipid flippases and Sfk1 are essential for the retention of ergosterol in the plasma membrane. Mol Biol Cell 32, 1374–1392.
Kock C, Arlt H, Ungermann C, Heinisch JJ (2016). Yeast cell wall integrity sensors form specific plasma membrane microdomains important for signalling. Cell Microbiol 18, 1251–1267.
Kock C, Dufrene YF, Heinisch JJ (2015). Up against the wall: Is yeast cell wall integrity ensured by mechanosensing in plasma membrane microdomains? Appl Environ Microbiol 81, 806–811.
Kurosaka G, Uemura S, Mochizuki T, Kozaki Y, Hozumi A, Suwa S, Ishii R, Kato Y, Imura S, Ishida N, *et al*. (2019). A novel ER membrane protein Ehg1/May24 plays a critical role in maintaining multiple nutrient permeases in yeast under high-pressure perturbation. Sci Rep 9, 18341.
Ladoux B, Mege RM (2017). Mechanobiology of collective cell behaviours. Nat Rev Mol Cell Biol 18, 743–757.
Laize V, Gobin R, Rousselet G, Badier C, Hohmann S, Ripoche P, Tacnet F (1999). Molecular and functional study of *AQY1* from *Saccharomyces cerevisiae*: Role of the C-terminal domain. Biochem Biophys Res Commun 257, 139–144.
Lanze CE, Gandra RM, Foderaro JE, Swenson KA, Douglas LM, Konopka JB (2020). Plasma membrane MCC/Eisosome domains promote stress resistance in fungi. Microbiol Mol Biol Rev 84, e00063–19.
Laz EV, Lee J, Levin DE (2020). Crosstalk between *Saccharomyces cerevisiae* SAPKs Hog1 and Mpk1 is mediated by glycerol accumulation. Fungal Biol 124, 361–367.
Lee J, Reiter W, Dohnal I, Gregori C, Beese-Sims S, Kuchler K, Ammerer G, Levin DE (2013). MAPK Hog1 closes the S. cerevisiae glycerol channel Fps1 by phosphorylating and displacing its positive regulators. Genes Dev 27, 2590–2601.
Lesage G, Bussey H (2006). Cell wall assembly in *Saccharomyces cerevisiae*. Microbiol Mol Biol Rev 70, 317–343.
Leskoske KL, Roelants FM, Martinez Marshall MN, Hill JM, Thorner J (2017). The stress-sensing TORC2 complex activates yeast AGC-family protein kinase Ypk1 at multiple novel sites. Genetics 207, 179–195.
Levin DE (2011). Regulation of cell wall biogenesis in *Saccharomyces cerevisiae*: the cell wall integrity signaling pathway. Genetics 189, 1145–1175.
Levin DE (2005). Cell wall integrity signaling in *Saccharomyces cerevisiae*. Microbiol Mol Biol Rev 69, 262–291.
Levin DE, Bartlett-Heubusch E (1992). Mutants in the *S. cerevisiae PKC1* gene display a cell cycle-specific osmotic stability defect. J Cell Biol 116, 1221–1229.
Luyten K, Albertyn J, Skibbe WF, Prior BA, Ramos J, Thevelein JM, Hohmann S (1995). Fps1, a yeast member of the MIP family of channel proteins, is a facilitator for glycerol uptake and efflux and is inactive under osmotic stress. EMBO J 14, 1360–1371.
Ma H, Snook LA, Kaminskyj SGW, Dahms TES (2005). Surface ultrastructure and elasticity in growing tips and mature regions of aspergillus hyphae describe wall maturation. Microbiology (Reading) 151, 3679–3688.
Madden K, Snyder M (1998). Cell polarity and morphogenesis in budding yeast. Annu Rev Microbiol 52, 687–744.
Martin H, Rodriguez-Pachon JM, Ruiz C, Nombela C, Molina M (2000). Regulatory mechanisms for modulation of signaling through the cell integrity Slt2-mediated pathway in *Saccharomyces cerevisiae*. J Biol Chem 275, 1511–1519.
Matsuki H, Goto M, Tada K, Tamai N (2013). Thermotropic and barotropic phase behavior of phosphatidylcholine bilayers. Int J Mol Sci 14, 2282–2302.
Merchan S, Bernal D, Serrano R, Yenush L (2004). Response of the *Saccharomyces cerevisiae* Mpk1 mitogen-activated protein kinase pathway to increases in internal turgor pressure caused by loss of Ppz protein phosphatases. Eukaryot Cell 3, 100–107.
Minc N, Boudaoud A, Chang F (2014). Mechanical forces of fission yeast growth. Curr Biol 24, 1436.
Mishra R, Minc N, Peter M (2022). Cells under pressure: How yeast cells respond to mechanical forces. Trends Microbiol 30, 495–510.
Mochizuki T, Kimata Y, Uemura S, Abe F (2015). Retention of chimeric Tat2-Gap1 permease in the endoplasmic reticulum induces unfolded protein response in *Saccharomyces cerevisiae*. FEMS Yeast Res 15, fov044.
Mollapour M, Piper PW (2007). Hog1 mitogen-activated protein kinase phosphorylation targets the yeast Fps1 aquaglyceroporin for endocytosis, thereby rendering cells resistant to acetic acid. Mol Cell Biol 27, 6446–6456.
Mollapour M, Shepherd A, Piper PW (2009). Presence of the Fps1p aquaglyceroporin channel is essential for Hog1p activation, but suppresses Slt2(Mpk1)p activation, with acetic acid stress of yeast. Microbiology (Reading) 155, 3304–3311.
Muir A, Roelants FM, Timmons G, Leskoske KL, Thorner J (2015). Down-regulation of TORC2-Ypk1 signaling promotes MAPK-independent survival under hyperosmotic stress. eLife 4, e09336.
Nagahama T, Abdel-Wahab MA, Nogi Y, Miyazaki M, Uematsu K, Hamamoto M, Horikoshi K (2008). *Dipodascus tetrasporeus* sp. nov., an ascosporogenous yeast isolated from deep-sea sediments in the Japan Trench. Int J Syst Evol Microbiol 58, 1040–1046.
Neeli-Venkata R, Diaz CM, Celador R, Sanchez Y, Minc N (2021). Detection of surface forces by the cell-wall mechanosensor Wsc1 in yeast. Dev Cell 56, 2856–2870.e7.
Niles BJ, Mogri H, Hill A, Vlahakis A, Powers T (2012). Plasma membrane recruitment and activation of the AGC kinase Ypk1 is mediated by target of rapamycin complex 2 (TORC2) and its effector proteins Slm1 and Slm2. Proc Natl Acad Sci USA 109, 1536–1541.
Nonaka H, Tanaka K, Hirano H, Fujiwara T, Kohno H, Umikawa M, Mino A, Takai Y (1995). A downstream target of *RHO1* small GTP-binding protein is *PKC1*, a homolog of protein kinase C, which leads to activation of the MAP kinase cascade in *Saccharomyces cerevisiae*. EMBO J 14, 5931–5938.
Orlean P (2012). Architecture and biosynthesis of the *Saccharomyces cerevisiae* cell wall. Genetics 192, 775–818.
Pattappa G, Zellner J, Johnstone B, Docheva D, Angele P (2019). Cells under pressure - the relationship between hydrostatic pressure and mesenchymal stem cell chondrogenesis. Eur Cell Mater 37, 360–381.
Peterson J, Zheng Y, Bender L, Myers A, Cerione R, Bender A (1994). Interactions between the bud emergence proteins Bem1p and Bem2p and rho-type GTPases in yeast. J Cell Biol 127, 1395–1406.
Philip B, Levin DE (2001). Wsc1 and Mid2 are cell surface sensors for cell wall integrity signaling that act through Rom2, a guanine nucleotide exchange factor for Rho1. Mol Cell Biol 21, 271–280.
Piao HL, Machado IM, Payne GS (2007). NPFXD-mediated endocytosis is required for polarity and function of a yeast cell wall stress sensor. Mol Biol Cell 18, 57–65.
Pruyne D, Bretscher A (2000). Polarization of cell growth in yeast. I. establishment and maintenance of polarity states. J Cell Sci 113, 365–375.
Riggi M, Niewola-Staszkowska K, Chiaruttini N, Colom A, Kusmider B, Mercier V, Soleimanpour S, Stahl M, Matile S, Roux A, Loewith R (2018). Decrease in plasma membrane tension triggers PtdIns(4,5)P2 phase separation to inactivate TORC2. Nat Cell Biol 20, 1043–1051.
Rispal D, Eltschinger S, Stahl M, Vaga S, Bodenmiller B, Abraham Y, Filipuzzi I, Movva NR, Aebersold R, Helliwell SB, Loewith R (2015). Target of rapamycin complex 2 regulates actin polarization and endocytosis via multiple pathways. J Biol Chem 290, 14963–14978.
Roelants FM, Baltz AG, Trott AE, Fereres S, Thorner J (2010). A protein kinase network regulates the function of aminophospholipid flippases. Proc Natl Acad Sci USA 107, 34–39.
Roelants FM, Breslow DK, Muir A, Weissman JS, Thorner J (2011). Protein kinase Ypk1 phosphorylates regulatory proteins Orm1 and Orm2 to control sphingolipid homeostasis in *Saccharomyces cerevisiae*. Proc Natl Acad Sci USA 108, 19222–19227.

Roelants FM, Torrance PD, Bezman N, Thorner J (2002). Pkh1 and Pkh2 differentially phosphorylate and activate Ypk1 and Ykr2 and define protein kinase modules required for maintenance of cell wall integrity. Mol Biol Cell 13, 3005–3028.

Roelants FM, Torrance PD, Thorner J (2004). Differential roles of PDK1- and PDK2-phosphorylation sites in the yeast AGC kinases Ypk1, Pkc1 and Sch9. Microbiology (Reading) 150, 3289–3304.

Sabir F, Loureiro-Dias MC, Soveral G, Prista C (2017). Functional relevance of water and glycerol channels in *Saccharomyces cerevisiae*. FEMS Microbiol Lett 364, fnx080.

Sakata KT, Hashii K, Yoshizawa K, Tahara YO, Yae K, Tsuda R, Tanaka N, Maeda T, Miyata M, Tabuchi M (2022). Coordinated regulation of TORC2 signaling by MCC/eisosome-associated proteins, Pil1 and tetraspan membrane proteins during the stress response. Mol Microbiol 117, 1227–1244.

Schaber J, Adrover MA, Eriksson E, Pelet S, Petelenz-Kurdziel E, Klein D, Posas F, Goksör M, Peter M, Hohmann S, Klipp E (2010). Biophysical properties of *Saccharomyces cerevisiae* and their relationship with HOG pathway activation. Eur Biophys J 39, 1547–1556.

Schmidt A, Bickle M, Beck T, Hall MN (1997). The yeast phosphatidylinositol kinase homolog TOR2 activates RHO1 and RHO2 via the exchange factor ROM2. Cell 88, 531–542.

Schmidt A, Schmelzle T, Hall MN (2002). The RHO1-GAPs SAC7, BEM2 and BAG7 control distinct RHO1 functions in *Saccharomyces cerevisiae*. Mol Microbiol 45, 1433–1441.

Schoppner P, Lutz AP, Lutterbach BJ, Bruckner S, Essen LO, Mosch HU (2022). Structure of the yeast cell wall integrity sensor Wsc1 reveals an essential role of surface-exposed aromatic clusters. J Fungi (Basel) 8, 379.

Sikorski RS, Hieter P (1989). A system of shuttle vectors and yeast host strains designed for efficient manipulation of DNA in *Saccharomyces cerevisiae*. Genetics 122, 19–27.

Siliciano PG, Tatchell K (1984). Transcription and regulatory signals at the mating type locus in yeast. Cell 37, 969–978.

Stradalova V, Stahlschmidt W, Grossmann G, Blazikova M, Rachel R, Tanner W, Malinsky J (2009). Furrow-like invaginations of the yeast plasma membrane correspond to membrane compartment of Can1. J Cell Sci 122, 2887–2894.

Straede A, Heinisch JJ (2007). Functional analyses of the extra- and intracellular domains of the yeast cell wall integrity sensors Mid2 and Wsc1. FEBS Lett 581, 4495–4500.

Suzuki A, Mochizuki T, Uemura S, Hiraki T, Abe F (2013). Pressure-induced endocytic degradation of the *Saccharomyces cerevisiae* low-affinity tryptophan permease Tat1 is mediated by Rsp5 ubiquitin ligase and functionally redundant PPxY motif proteins. Eukaryot Cell 12, 990–997.

Tabuchi M, Audhya A, Parsons AB, Boone C, Emr SD (2006). The phosphatidylinositol 4,5-biphosphate and TORC2 binding proteins Slm1 and Slm2 function in sphingolipid regulation. Mol Cell Biol 26, 5861–5875.

Tamás MJ, Luyten K, Sutherland FC, Hernandez A, Albertyn J, Valadi H, Li H, Prior BA, Kilian SG, Ramos J, *et al*. (1999). Fps1p controls the accumulation and release of the compatible solute glycerol in yeast osmoregulation. Mol Microbiol 31, 1087–1104.

Thorsen M, Di Y, Tängemo C, Morillas M, Ahmadpour D, Van der Does C, Wagner A, Johansson E, Boman J, Posas F, *et al*. (2006). The MAPK Hog1p modulates Fps1p-dependent arsenite uptake and tolerance in yeast. Mol Biol Cell 17, 4400–4410.

Uemura S, Mochizuki T, Amemiya K, Kurosaka G, Yazawa M, Nakamoto K, Ishikawa Y, Izawa S, Abe F (2020). Amino acid homeostatic control by TORC1 in *Saccharomyces cerevisiae* under high hydrostatic pressure. J Cell Sci 133, jcs245555.

Usami Y, Uemura S, Mochizuki T, Morita A, Shishido F, Inokuchi J, Abe F (2014). Functional mapping and implications of substrate specificity of the yeast high-affinity leucine permease Bap2. Biochim Biophys Acta 1838, 1719–1729.

Vay HA, Philip B, Levin DE (2004). Mutational analysis of the cytoplasmic domain of the Wsc1 cell wall stress sensor. Microbiology (Reading) 150, 3281–3288.

Wilk S, Wittland J, Thywissen A, Schmitz HP, Heinisch JJ (2010). A block of endocytosis of the yeast cell wall integrity sensors Wsc1 and Wsc2 results in reduced fitness in vivo. Mol Genet Genomics 284, 217–229.

Winter R (2002). Synchrotron X-ray and neutron small-angle scattering of lyotropic lipid mesophases, model biomembranes and proteins in solution at high pressure. Biochim Biophys Acta 1595, 160–184.

Winzeler EA, Shoemaker DD, Astromoff A, Liang H, Anderson K, André B, Bangham R, Benito R, Boeke JD, Bussey H, *et al*. (1999). Functional characterization of the S. cerevisiae genome by gene deletion and parallel analysis. Science 285, 901–906.

Yamaguchi M, Taguchi M, Uematsu K, Takahashi-Nakaguchi A, Sato-Okamoto M, Chibana H (2021). Sandwich freezing device for rapid freezing of viruses, bacteria, yeast, cultured cells and animal and human tissues in electron microscopy. Microscopy (Oxf) 70, 215–223.

Yamaguchi M, Takahashi-Nakaguchi A, Uematsu K, Taguchi M, Sato-Okamoto M, Chibana H (2021). Rapid freezing using sandwich freezing device for good ultrastructural preservation of biological specimens in electron microscopy. J Vis Exp.173, e62431.

Yoshida S, Bartolini S, Pellman D (2009). Mechanisms for concentrating Rho1 during cytokinesis. Genes Dev 23, 810–823.

Yoshino D, Funamoto K, Sato K, Kenry, Sato M, Lim CT (2020). Hydrostatic pressure promotes endothelial tube formation through aquaporin 1 and Ras-ERK signaling. Commun Biol 3, 152.